DIACYLGLYCEROL KINASE THETA AT THE SYNAPSE: A ROLE FOR THE METABOLISM OF DAG IN SYNAPTIC VESICLE RECYCLING

By

Hana L. Goldschmidt

A dissertation submitted to The Johns Hopkins University in conformity with the requirement of the degree of Doctor of Philosophy

Baltimore, MD

March 2015

ABSTRACT

In the mammalian nervous system, synaptic transmission relies on coordinated coupling of synaptic vesicle (SV) exocytosis and endocytosis. While much attention has focused on characterizing the proteins involved in SV recycling, the roles of membrane lipids and their metabolism remain poorly understood. Diacylglycerol, a major signaling lipid produced at synapses during synaptic transmission, is regulated by diacylglycerol kinase (DGK). Of the ten known mammalian DGK isoforms, DGKθ is one of the least studied DGK isoforms found in the brain with no known function to date. **The goal of this study aimed to identify and characterize the function of DGKθ in the mammalian CNS.** This thesis describes the first functional role for DGKθ in the mammalian central nervous system in facilitating recycling of presynaptic vesicles at excitatory synapses. Using an optical reporter, we found that acute and chronic deletion of DGKθ attenuated the recovery of SVs following neuronal stimulation. Rescue of recycling kinetics required DGKθ kinase activity. Our data establish a role for DGK catalytic activity and its byproduct, phosphatidic acid, at the presynaptic nerve terminal in facilitating SV recycling. Together these data suggest DGKθ supports synaptic transmission during periods of elevated neuronal activity.

DISSERTATION REFEREES

Graduate Advisor: **Daniel M. Raben, Ph.D.,** Professor, Department of Biological Chemistry

Graduate Advisor: **Richard L. Huganir, Ph.D.,** Professor, Department of Neuroscience

ACKNOWLEDGEMENTS

This dissertation is the product of six years of challenging and exciting research that exemplifies the multidisciplinary nature of the BCMB program at the Johns Hopkins University School of Medicine. With the strong scientific foundation provided by BCMB curriculum, two incredible thesis advisors and the support of many colleagues, friends and family I was able to pursue my passion for biochemistry and follow my curiosity of how cells work towards pursuing a PhD. I would like to dedicate this dissertation to all of these wonderful people who have helped me throughout the many stages of this journey and continue to support me to evolve into the scientist and woman I am today. Thank you.

I am particularly grateful to my two thesis advisors, Dr. Daniel Raben and Dr. Richard Huganir. Their combined mentorship, collaborative nature, support and encouragement provided me with the unique opportunity to "follow the data" from lipid biochemistry to synapse function. From their example and guidance, I learned the "mental gymnastics" of how to critically think about and pursue scientific questions. A special thanks goes to Dan for giving me a home in the Department of Biological Chemistry. I admire and have been inspired by his energy and enthusiasm for science, metabolism, and data. He has given me invaluable guidance and support every step of the way. Dan expanded my scientific world, from New Hampshire to Argentina, for which I am eternally grateful. I would also like to thank Dr. Becky Tu-Sekine, an alumni of the Raben Lab, who has helped me from the beginning when I was first rotating in the Raben lab. She is the expert on everything DGKθ, a brilliant lipid biochemist, colleague and friend.

A special thanks to Dr. Victor Anggono who helped me get this project going with a running start. He is an incredible scientist, and I am truly fortunate to have been able to work with him so closely at the beginning of my PhD. It was through this productive collaboration with Victor, when he was a postdoc in the Huganir lab, that catapulted my project into the wonderful world of neuroscience. I am truly grateful to Rick and all of the members of his lab, past and present, that accepted me graciously and enthusiastically into their lab during my third year of graduate school. Their expertise, insight, stimulating and fun lab environment was key to the success of my project. A special thanks to Dr. Lenora Volk who performed all of the electrophysiology analysis on the DGKθ KO mice. I am grateful to have had the opportunity to work so closely with such a brilliant scientist and friend.

I would also like to thank all the members of Team Canada: Drs. Natasha K. Hussain, Yuko Oku, Graham Diering, David Benavides, Alyssa Toda and Han Tan. It has been a privilege to be able to work so closely with such an outstanding, fun, and creative group of scientists. I am especially grateful to Graham and Natasha, the Chief Ministers of Team Canada, for all their scientific training, expertise, and wisdom. I truly admire them as scientists, mentors, colleagues and friends. Thanks to Brian Loeper and Rebecca White for all their hard work managing the mice and more recently, the Huganir lab. The success of this project has been contingent on Brian's musical talent, which got the DGKθ mice colony rolling. A very special thanks to Lisa Hamm, Monica Coulter, and Richard Johnson, who are essential members of the Huganir Lab.

I would also like to thank my thesis committee, Dr. Seth Margolis, Dr. Carolyn Machamer and Dr. Michael Wolfgang, for all of their valuable insight and guidance over

the course of my PhD. I am especially grateful to the generosity, support, and friendship I received from Seth and the entire Margolis lab. Like Dan and Rick, Seth leads by example and is role model of a scientist and collaborator. I am grateful for the time he spent helping me with presentations and writing (including reading various versions of this thesis). The door was always open to his office and lab to chat about everything from cool data to Jewish-Indian weddings. His mentorship helped me build confidence in myself as a scientist, and for that I am very grateful.

I would like to especially thank my undergraduate research mentor, Dr. Chris Craney and organic chemistry professor, Dr. Tetsuo Otsuki, for recognizing my potential to become a scientist when I first arrived at Occidental College. They both fueled my enthusiasm for biochemistry by making science fun, applicable, challenging, and relevant to everyday life. They introduced me to the world of biochemistry research, which I subsequently fell in love with and have been pursuing ever since.

I would also like to thank Dr. Kevin Shannon and the members of his laboratory at UCSF. In the Shannon lab I had the amazing opportunity to work with talented physician scientists and basic biochemistry scientists. In the Shannon lab I saw for the first time the union of basic biochemistry research and medicine, and learned how valuable collaboration between the two could be used not only to transform treatment of deadly diseases, but also to expand our understanding of how the human body works on a molecular level.

Finally, I would also like to thank my mother, Marilee Stark, and sister, Liliana Goldschmidt, who without their emotional and financial support, I would not be here. I am truly fortunate to have such a solid base in my life. Like Dr. Craney and Dr. O, they

too recognized my potential long before I did, and for that I will be eternally grateful. The scientist and woman I am today is a product of their guidance, friendship, laughter, insight, style, politics, and wisdom. They encouraged me to stay on my path toward being a scientist.

Many thanks to the BCMB office and the Department of Biological Chemistry for their support during my graduate career, especially Sharon Root and Lesley Brown. This work was supported by RO1N5077923 (DMR), RO1N5036715 (RLH) and the John T. Reid Charitable Trusts (VA).

TABLE OF CONTENTS

LIST OF FIGURES

Chapter 1

Chapter 3

Chapter 4

Chapter 5

Chapter 6

LIST OF ABBREVIATIONS

ACSF	artificial cerebrospinal fluid
APV	D,L-2-amino-5-phosphonovaleric acid
C-terminus	carboxyl terminus
CNQX	6-cyano-7-nitroquinoxaline-2,3-dione
CNS	central nervous system
DAG	Diacylglycerol
DIV	days *in vitro*
DGK	diacylglycerol kinase
HEK 293T	human embryonic kidney cell 293 with T antigen
KO	knockout
NT	neurotransmitter
N-terminus	amino terminus
P	postnatal
PH	Pleckstrin Homology domain
PPR	paired-pulse ratio
PPF	paired-pulse facilitation
PSD	postsynaptic density
PtdIns	phosphatidyl Inositol
PtdIns(4,5)P_2	Phosphatidylinositol-4,5-bisphosphate
PtdOH	Phosphatidic Acid
PTX	picrotoxin
SC-CA1	Schaffer collateral-cornu ammonis 1 pyramidal neurons

shRNA	short hairpin RNA
sypHy	synaptophysin-pHluorin
TTX	tetrodotoxin
WT	wild-type

CHAPTER 1.

INTRODUCTION

Basic brain function depends on communication between neurons. The process of sending a message from one neuron to its neighbor occurs at specialized sites, called synapses. The arrival of an action potential to the presynaptic nerve terminal initiates this communication process by stimulating the release of neurotransmitter-filled SVs from the presynaptic terminal. The neurotransmitters then travel across the synaptic cleft where they bind to and activate receptors in the postsynaptic membrane, thereby initiating a new signaling cascade to propagate the message into the neighboring neuron. Understanding the molecular mechanisms that regulate this communication, which, in turn, dictate higher brain function, is critical for understanding nervous system function in health and disease.

Despite making up half of the dry weight of the human brain, membrane lipids have only recently begun to emerge as important modulators of neuronal function(*1*). Initially thought of as structural building blocks of membranes or high energy sources of cellular fuel, several studies have now identified many important signaling roles for membrane lipids in basic synaptic function as well as neurological disorders(*2-4*). Like other soluble second messengers, signaling lipids are maintained at very low concentrations in a resting cell. Since the availability and abundance of signaling lipids is dictated by the enzymes that mediate their generation and metabolism in membranes, lipid metabolizing enzymes are not surprisingly emerging as important regulators of neuronal function(*3*, *5*). While we are still at the early stages of understanding the neuronal functions of membrane lipids and their metabolic enzymes, much of what we know comes from studies examining how these molecules regulate the important synaptic vesicle cycle.

1.1 Synaptic transmission and the synaptic vesicle cycle

The ability of neuronal cells to transmit information rapidly and reliably is critical for the proper function of the nervous system (*6*). This is achieved in part through the synaptic vesicle (SV) cycle, a tightly regulated process that efficiently recycles and reuses SVs during neuronal firing (**Figure 1.1)** (*7*, *8*). The cycle is initiated by the arrival of an action potential to the presynaptic terminal, which triggers Ca^{2+}-mediated fusion of SVs with the plasma membrane (exocytosis) and release of neurotransmitters into the synaptic cleft. SVs are then taken back up into the nerve terminal via endocytosis, refilled with neurotransmitters and recycled for another round of release.

The efficiency of neurotransmission is in part defined by the limited supply of 100-300 SVs available within each nerve terminal (*8*, *9*). *De novo* synthesis of SV can take upwards of hours to days for a new SV made in the cell soma to reach the synapse, a process far too slow to sustain neurotransmitter release and transmission, which occurs several orders of magnitude faster (milliseconds to minutes) (*10*). Therefore, neurons rely on local recycling of SVs within the bouton to maintain neurotransmission. This becomes particularly critical during periods of elevated neuronal activity, where multiple SVs fuse with the membrane over a short period of time (*11*). SV recycling is essential for neuronal function, and its dysregulation may contribute to several neurological and psychiatric disorders (*8*, *12*).

Figure 1.1

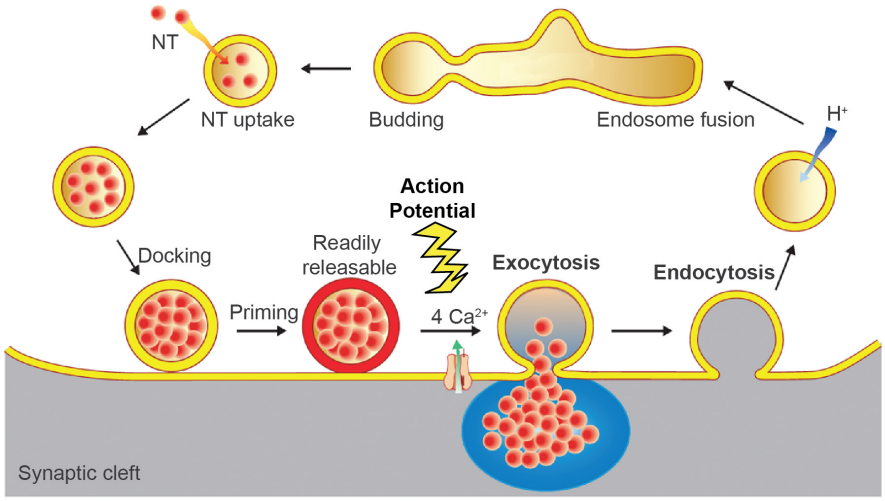

Figure 1.1 The synaptic vesicle cycle. Schematic of the basic steps of the synaptic vesicle (SV) cycle at central nerve terminals. The cycle begins with the arrival of an action potential to the presynaptic nerve terminal. Depolarization of the presynaptic membrane opens voltage-gated Ca^{2+} channels. The resulting influx of Ca^{2+} ions triggers exocytosis of SVs and release of neurotransmitters (red) into the synaptic cleft, where they to bind receptors on the postsynaptic membrane and propagate the signal (postsynaptic membrane not shown). The SV membrane is then recovered from the plasma membrane via endocytosis, reacidified and filled with neurotransmitters, and recycled back to either the recycling pool of vesicles or the membrane fore another round of release. *Figure modified from* (*13*, *14*)

Despite being one of the most well-studied cellular processes, the mechanisms that mediate the steps of the SV cycle, particularly those involved in endocytosis, remain a matter of debate. To date, four mechanisms of SV endocytosis have been described: (1) clathrin-mediated endocytosis (CME), (2) activity-dependent bulk endocytosis (ADBE) (*11*), (3) kiss-and-run(*13*), (4) and most recently ultra-fast-endocytosis(*15*). These pathways are differentially utilized depending on the strength and duration of neuronal activity, as well as their molecular machinery, speed and capacity for membrane retrieval. For the purpose of this thesis, CME and ADBE, are the most well understood pathways that predominant SV endocytosis during mild or strong neuronal firing, respectively, and are summarized below in **Figure 1.2** (*16*).

Figure 1.2

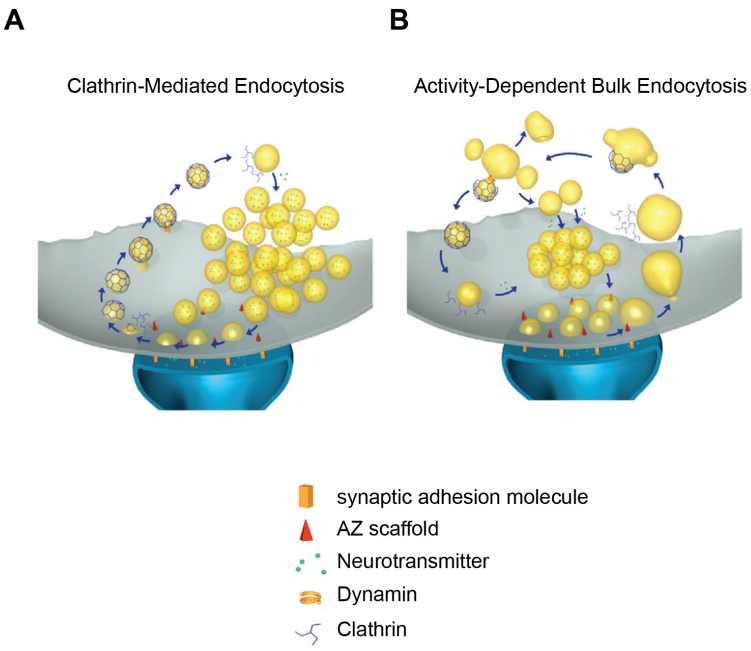

Figure 1.2 Predominant mechanisms of SV recycling. (A) Clathrin-mediated endocytosis, the dominant mechanism for vesicle retrieval during mild neuronal activity, occurs on the scale of 10-30s. Following complete fusion of the SV with the plasma membrane, SV membrane and protein components are recovered directly from the plasma membrane via formation of clathrin coated vesicles. These vesicles are then pinched off from the membrane by the action of dynamin, uncoated, and then refilled with neurotransmitters, and trafficked to the recycling pool of SVs or back to the membrane. (B) Activity-dependent bulk endocytosis is dominant mechanism of SV endocytosis during elevated neuronal activity. This mechanism involves retrieval of large areas of synaptic membrane (bulk endocytic structures). SVs then bud off from the endosome, via clathrin-dependent and clathrin-independent mechanisms. *Figure modified from* (*10*)**.**

1.2 Role for lipids in neurotransmission

In the SV cycle, exocytosis of vesicles is tightly linked with endocytosis, and variations in the number of vesicles and/or defects in the refilling of vesicles will affect the amount of neurotransmitter available for release (*13*). While previous studies outlined an array of proteins involved in the SV cycle, the lipid composition of presynaptic membranes also plays an active role in the regulation of synaptic vesicle recycling (*7*, *17*, *18*). However, the enzymes involved in lipid metabolism that is important for regulating vesicle recycling are not well understood (*2*, *3*, *5*).

Of the membrane lipids that have been studied, phosphoinositides have the most well established role in this cycle (*2*, *3*). Phosphatidylinositol-4,5-bisphosphate (PtdIns(4,5)P_2), modulates both SV exo- and endocytosis by recruiting and activating proteins required for theses pathways (e.g. synaptotagmin I (*2*, *19*), clathrin adaptor proteins AP2 and dynamin-1 (*7*, *20*, *21*)) to the presynaptic membrane. The emerging role of PtdIns(4,5)P_2 in the regulation of the SV cycle inherently implicates the enzymes that control the abundance of this lipid in synaptic membranes. Consistent with this notion, genetic deletion of the lipid kinase (phosphatidylinositol phosphate kinase type Iγ, PIPK1γ) (*7*), or phosphatase (synaptojanin 1) (*17*, *18*) that mediate the generation and metabolism of PtdIns(4,5)P_2 respectively, resulted in multiple synaptic defects, including impaired SV recycling kinetics. In addition to a role for the intact PtdIns(4,5)P_2, metabolism of this lipid via a phospholipase C to generate diacylglycerol (DAG) is also implicated in synaptic function (*7*, *22*). DAG may play at least three roles in the SV cycle. First, DAG binds Munc13-1and mediates its role in the priming of SVs for exocytosis, a function that is absolutely required for SV fusion during spontaneous and

evoked synaptic transmission (*23-26*). Second, DAG activates PKC, which phosphorylates and thereby regulates the activities of presynaptic SNARE complex proteins (Munc-18, SNAP-25) (*7*, *27*, *28*). Finally, termination of DAG signaling through its phosphorylation by DAG kinases (DGKs) results in the production of phosphatidic acid (PtdOH), an acidic phospholipid which can act as a signaling molecule itself as well as a precursor for the generation of phosphatidylinositol, and ultimately PtdIns(4,5)P_2 (*29-31*).

Figure 1.3

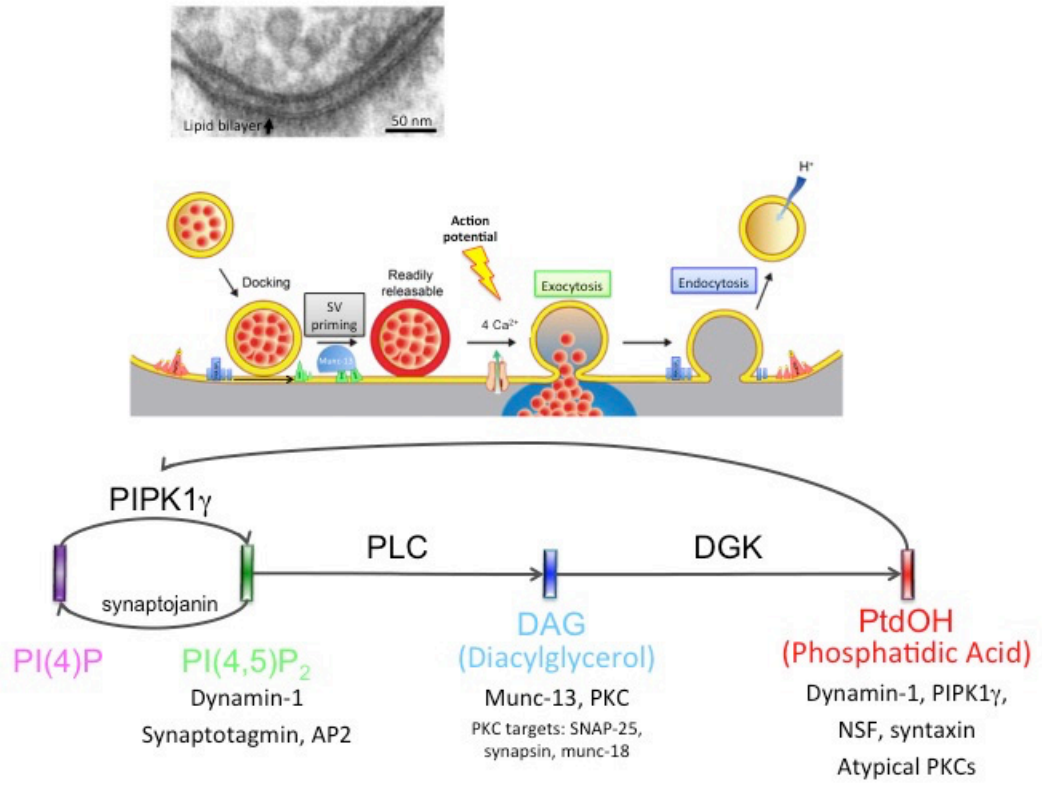

Figure 1.3 Lipid regulation of the synaptic vesicle cycle Top, electron micrograph of hippocampal CA1 synapse showing the presynaptic membrane and the lipid bilayer (arrow). Middle, detailed schematic of the SV cycle shown in Figure 1.1, highlighting the steps where the lipids are known to play regulatory roles. Bottom, lipid kinases (PIPK1γ, DGK), phosphatases (synaptojanin), and lipases (PLC), regulate the levels of PtdIns (PI lipids), DAG, and PtdOH. *Figure modified from* (*10*)**.**

1.3 Diacylglycerol kinases

DGKs constitute a large family of lipid kinases that are abundant in CNS (*22*, *29*). The fact that all ten DGK isoforms (α, β, γ, δ, ε, ζ, η, θ, ι and κ) are expressed in the mammalian brain lends strong support for the concept that these enzymes are required to support brain function. Indeed, several functional studies have implicated individual DGK isoforms in modulating spine dynamics, SV release probability, neuronal plasticity and neurological disorders (β, ζ, ι, ε, η) (*32-36*). However, at present there are no reports that examine the cellular function of DGKθ in the mammalian central nervous system. Given the importance of PtdIns(4,5)P_2-DAG mediated signaling at presynaptic terminals, and the fact that the *C. elegans* DGK-1, an ortholog of DGKθ, modulates neurotransmitter release (*37*), we hypothesized that DGKθ may have an important role in controlling SV recycling.

The data presented in the study presented in this thesis show DGKθ plays an important role in modulating SV recycling in mammalian cortical neurons. Both shRNA-mediated knockdown of DGKθ and neurons derived from DGKθ knock-out mice exhibit a decreased rate of synaptic vesicle endocytosis compared to control neurons. Importantly, this defect in SV recycling is rescued by ectopic expression of enzymatically active DGKθ, but not a kinase-dead enzyme. Our data are the first to establish a role for DGKθ kinase activity in the regulation of SV recycling, and suggest that DGKθ supports synaptic transmission during periods of sustained neuronal activity.

CHAPTER 2.

MATERIALS AND METHODS

2.1 Animals

Wild-type (WT) and DGKθ knock-out (KO) mice used for this research were made from heterozygous Dgkq$^{tm1a(KOMP)Wtsi}$ generated by the trans-NIH Knock-Out Mouse Project (KOMP) and obtained from the KOMP Repository (www.komp.org). NIH grants to Velocigene at Regeneron Inc. (U01HG004085) and the CSD Consortium (U01HG004080) funded the generation of gene-targeted ES cells for 8500 genes in the KOMP Program and archived and distributed by the KOMP Repository at UC Davis and CHORI (U42RR024244). For more information or to obtain KOMP products go to www.komp.org or email service@komp.org. Sprague Dawley rats were used for E18 hippocampal and cortical cultures. All animals were treated in accordance with the Johns Hopkins University Animal Care and Use Committee guidelines. (https://www.komp.org/faq.php#faq11)

2.2 Reagents

Imaging reagents: TTX, DL-AP5, and CNQX (Tocris), were resuspended with water to make 1000x stock solutions (1 mM, 50 mM, 10 mM, respectively), aliquots were stored at -20°C until use. Bafilomycin A1 (Calbiochem) was resuspended in DMSO to make 1mM stock solution, aliquots were stored at -20°C until use. Antibodies: mouse anti-DGKθ, DGKι, DGKγ from BD biosciences, chicken anti-MAP2 (Novus), mouse anti-PSD-95 (NeuroMab), guinea pig anti-vGlut1 (Synaptic systems), mouse β-Tubulin (Sigma), rabbit anti-GluR1 (RLH lab), rabbit anti-dsRed (Clontech), chicken anti-GFP (Abcam). IRDye-conjugated secondary antibodies were used for infrared imaging (Odyssey; LICOR).

2.3 DNA constructs (Molecular Biology)

shRNA-knockdown and rescue plasmids. Complementary primers containing DGKθ or control shRNA (Ctrl) sequences were annealed and cloned into *Sac*I and *Xho*I sites of pSuper vector and driven by H1 RNA polymerase III promoter. Ctrl shRNA sequence was specific for luciferase. shRNA targeting sequences: DGKθ-shRNA (*38*), 5'-GTGTACATTTGGACGTCTA -3'; luciferase shRNA, 5'-CGCTGAGTACTTCGAAATGTC -3'. For rescue experiments, human DGKθ or DGKθ-kinase dead (DGKθ-kd, point-mutation G648A in kinase domain (*39*)) was subcloned into pRK5-Myc between *Sal*I and *Not*I restriction sites and driven by CMV promoter (^{Myc}DGKθ and ^{Myc}DGKθ-kd, respectively). Other DNA plasmids used: synaptophysin-pHluorin (CMV::SypHy A4) was obtained from Addgene (plasmid 24478).

2.4 Lentivirus

Control and DGKθ-shRNA were subcloned into FuGW lentiviral vector and lentivirus was produced as described previously(*40*). Briefly, HEK 293 cells were transfected with FuGW, d8.9, VSV-G, using lipofectamine 2000. Cells were treated with sodium butyrate 18hrs post-transfection, Virus was collected 8hrs, and 24hrs post treatment. Virus was concentrated, and resuspended in NB, aliquots were frozen and stored at -80C.

2.5 Neuronal Cell Culture

Cortical neurons from E18 rat pups were plated onto poly-L-lysine coated dishes or 18mm coverslips in Neurobasal growth medium supplemented with 2%B27, 2 mM Glutamax, 50 U/mL penicillin, 50 µg/mL streptomycin, and 5% Horse serum. After 3-4

days *in vitro* (DIV) neurons were treated with FDU diluted into growth medium supplemented as above but with 1% horse serum. Neurons were then maintained in glial-conditioned growth medium (1% serum) and fed twice a week. Mouse neuronal cultures were prepared as described about from age-matched E16-E18 WT and homozygous DGKθ KO pups.

2.6 Determination of DGKθ half-life

Cyclohexamide (20 mg/mL) was added to N2a and 3T3 cells 24 h after cells were seeded in 12W plates. Cells were collected at 0, 2, 4, 6, 24, 48, and 72 h and whole-cell lysates were prepared for western blotting analysis. The relative amount of DGKθ protein was determined with densitometry (Odyssey infrared systems, LiCor Biosciences) and normalized to α-GAPDH or α-tubulin. Curve fitting was done using Prism 5 software (GraphPad Software, San Diego CA).

2.7 Glutamate release assay.

For these experiments, rat cortical neurons were infected on DIV 8 with lentiviral particles containing either control or DGKθ-shRNA. ~1 week later (DIV 14-15) cells were assayed for extracellular glutamate release following depolarization with high K+ buffer. Briefly, cells were washed two times with ACSF (122.5 mM NaCl, 2.5 mM KCl, 2 mM $CaCl_2$, 2 mM $MgCl_2$, 30 mM D-glucose, 25 mM Hepes, pH 7.4) and then depolarized for 1 m with 90 mM KCl (ACSF with 90 mM KCl, 35 mM NaCl). Samples were removed after 10, 20 and 60 s of stimulation and extracellular glutamate was quantitated using the Amplex Red glutamate oxidase assay (Invitrogen) as described by

the manufacturer. After each experiment, neurons were harvested in lysis buffer and lysates were analyzed by western blot to determine knockdown efficiency. 1 μM tetrodotoxin (TTX) and 100 μM TBOA was included in ACSF and 90 mM KCl buffers.

2.9 Synaptic vesicle recycling assay with synaptophysin-pHluorin

Transfection. Neurons were transfected DIV 8-11 using lipofectamine 2000 (Invitrogen) and sypHy live-cell imaging was performed DIV 14-20. Concentration of DNAs used are as follows: 1 μg sypHy, 0.4 μg mCherry, 0.2 μg empty vector (pRK5-Myc) or ^{Myc}DGKθ, or ^{Myc}DGKθ –kd; for shRNA-knockdown 1 μg of control (shLuc) or DGKθ-specific shRNA (shLuc and sh#1, respectively) was also included.

Live-cell imaging. Coverslips containing neurons were mounted into a custom-built perfusion and stimulation chamber which held at 37°C on the heated microscope stage. Healthy, transfected neurons were identified by mCherry expression. During image acquisition, cells were continuously perfused at 0.5-1.0 mL/min with ACSF. Neurons were imaged through a 40x, oil objective (N.A= 1.6x) using a Zeiss spinning-disk confocal microscope. Fluorescence was imaged at 488 nm excitation and collected through a 505-550 nm filter and mCherry signal was imaged at 561 nm excitation and 575-615 nm emission. Images were acquired at a rate of 1 frame per 2 seconds. For KCl stimulation, 1 μM TTX was included in ACSF and high K+ buffer (ACSF with 50 mM KCl, 75 mM NaCl). Cells were perfused for 30 seconds with ACSF to obtain a baseline recording, then switched to high K+ buffer for 1 minute, and returned to ACSF for the reminder of imaging. For field stimulation, 10uM 6-cyano-7-nitroquinoxaline-2,3-dione

(CNQX) and 50uM D,L-2amino-5-phosphonovaleric acid (AP5) were included in the recording buffer instead of TTX. Action potentials were evoked at 10 or 50 Hz (100 mA, 1 ms pulse width, delivered using platinum wires embedded in the imaging chamber). Images were analyzed in ImageJ (http://rsb.info.nih.gov/ij/) using the time-series plugin (http://rsb.info.nih.gov/ij/plugins/time-series.html).

2.10 Immunocytochemistry

Neurons were rinsed with PBS and fixed for 15 minutes at room temperature in PBS containing 4% paraformaldehyde (PFA) and 4% sucrose. Cells were washed 3 times and permeabilized with 0.25%TX-100 in PBS for 10 minutes. Neurons were then blocked with 10% BSA serum in PBS for 1hr at 37^{o}C and incubated in primary antibodies in PBS containing 3% BSA at room temperature. Neurons were washed 5 times before they were incubated with fluorescently labeled secondary antibodies (goat conjugated Alexafluor 647, 568, or 488). Following 5 final washes with PBS, coverslips and mounted onto glass slides using Fluoromount-G (Southern Biotech). Images were obtained using a 510-laser scanning confocal microscope (Zeiss).

2.11 DGK activity assay

Assay was performed as described previously (*41*). Large unilamellar vesicles were prepared on the day of assay as follows: stock lipids were combined, dried under nitrogen and stored under vacuum at 4° C for 2-20 hours to remove residual $CHCl_3$. Lipid films were rehydrated in DGK assay buffer (55 mM Hepes, 100 mM NaCl) for 30 min at 40°C with occasional vortexing and sonication (30 seconds, Branson Sonicator). Vesicles were

formed at 37-40C by extrusion through a 0.1μm polycarbonate membrane using an Avanti mini extruder per manufacturer instructions. Lipid composition was POPC:POPE:POPS:DOG at mole fractions of 26:51:15:8, respectively. 5μg of S1 fractions were added to the vesicles and reactions were incubated 30 min at 37C without agitation. The final assay contained: 1.2 mM total lipid in 50 mM Hepes pH 7.5, 1 mM DTT, 1.5 mM $MgCl_2$, 1 mM [γ^{32} P]ATP (specific activity = $2.5x10^5$ cpm/nmol ATP). Reactions were terminated by addition of chloroform/methanol/1M NaCl (1:2:0.8) (v:v), and phases separated by addition of 1 ml each of $CHCl_3$ and 1M NaCl. The organic phase was washed with 2 ml of 1M NaCl, dried under nitrogen gas, resuspended in $CHCl_3$:MeOH (95:5) and spotted onto a silica gel 60 TLC plate. Phosphatidic acid (PtdOH) was separated from other lipids with chloroform:acetone:methanol:acetic acid:water (10:4:3:2:1) (v:v). The amount of [γ^{32}P]PtdOH was measured by liquid scintillation spectrophotometry in a Wallac 1410 liquid scintillation counter. DGK activity was quantified as nmol PtdOH min^{-1} μg^{-1} of protein. Assay conditions used in these experiments are routinely used to measure DGK activity of purified forms of DGKθ, DGKζ, and DGKδ (personal communication from Becky Tu-Sekine). By excluding calcium from the DGK assay buffer, we minimized activity measured in cell fraction from the type I DGK isoforms (α, β, and γ).

2.12 PSD preparation

Forebrain or whole brain was isolated from adult mouse and frozen on dry ice. Brain was thawed in homogenization buffer (320 mM sucrose, 5 mM sodium pyrophosphate, 1 mM EDTA, 10 mM HEPES pH 7.4, 200 nM okadaic acid, protease inhibitor cocktail

(Roche)) and homogenized 30 times in glass homogenizer. The homogenate was centrifuged at 800xg for 10 minutes at 4°C to yield P1 and S1. S1 was further centrifuged at 10,000xg for 20 minutes at 4°C to yield P2 and S2. P2 was layered on top of a sucrose gradient composed of 0.8, 1, 1.2 mM sucrose buffers, respectively, containing protease and phosphatase inhibitors. The gradient was centrifuged 82,500 xg for 2hrs at 4°C . The layer containing synaptosomes (between 1 and 1.2mM sucrose) was isolated, diluted with 10mM Hepes buffer, pH 7.4, and synaptosomes were pelleted by centrifugation at 150,000 x g for 30 minutes at 4°C. Synaptosomal pellet (SYN) was resuspended in 50mM HEPES pH 7.4, mixed with an equal volume of 1% triton X-100, and incubated with agitation at 4°C for 15 minutes. The PSD was generated by centrifugation at 32,000xg for 20 minutes at 4°C. The final PSD pellet was resuspended in 50mM HEPES pH 7.4 followed by protein quantification and western blot.

2.13 Electron microscopy

These experiments were done in collaboration with Michael Delannoy and the Johns Hopkins University School of Medicine Microscope Facility (http://www.hopkinsmedicine.org/micfac/) and Dr. Shu-Ling Chiu, a postdoctoral fellow in the Huganir lab. M.D. performed post-fixation processing of samples, S.H.C. perfused mice for hippocampal sections. H.L.G performed imaging acquisition and analysis. For analysis of synapses in hippocampal CA1 neurons, age-matched DGKθ WT and KO mice (6mo old) were anesthetized with avertin (0.03ml/g) then perfused with phosphate buffer (PB, 37°C see recipe below) followed by ~100 mL of the fixative solution (2.0% glutaraldehyde, 2.0% paraformaldehyde (freshly prepared form EM grade prill form),

100 mM sodium cacodylate and 3 mM $MgCl_2$, pH 7.4 at 4°C). Animals were perfused at ~7-8 mL/min. Brain tissue was removed and fixed in the same solution overnight at 4°C. 1 mm thick coronal sections that contained the hippocampal CA1 were cut down to 3 mm^3 pieces for further processing. Following buffer rinse containing 3% sucrose, samples were post-fixed in 1.5% potassium ferrocyanide ($K_4Fe(CN)_6$) reduced 2% osmium tetroxide (OsO_4) in 100mM sodium cacodylate with 3 mM $MgCl_2$ for 2 h on ice in the dark. After a brief rinse in 100 mM Maleate buffer containing 3% sucrose, tissue sections were placed in 2% uranyl acetate in maleate/sucrose (0.22 μm filtered) for 1 h at 4°C with slow rocking in the dark. Following en-bloc staining cells were dehydrated through a graded series of ethanol, transferred through propylene oxide and were embedded in Eponate 12 (Pella) and cured at 60°C for two days. Sections were cut on a Riechert Ultracut E with a Diatome Diamond knife. 80 nm sections were picked up on formvar coated 1 x 2 mm copper slot grids and stained with uranyl acetate followed by lead citrate. Grids were viewed on a Hitachi 7600 TEM operating at 80 kV and digital images captured with an XR50, 5 megapixel CCD camera (AMT).

WT and DGKθ KO neurons grown on 18mm coverslips were transferred to 35 mm tissue culture dishes (Falcon 3001) and rinsed two times with warm ACSF (37°C), then fixed with 1.3% glutaraldehyde in 66 mM sodium cacodylate containing 3 mM $CaCl_2$ pH 7.2 (~300 mOsmols) for 1 hr. at room temperature on a slow rocker. After a 30 min buffer rinse (100 mM sodium cacodylate with 2% sucrose and 3 mM $CaCl_2$), cells were post-fixed in 1% OsO_4 reduced with 1.5% $K_4Fe(CN)_6$ in 100 mM sodium cacodylate with 3 mM $CaCl_2$ at 4°C for 2 hrs in the dark. Samples were then rinsed with dH_2O and en-bloc stained with 0.5% uranyl acetate (0.22 um filtered, aq.) for 1 hr in the dark.

Plates were dehydrated in a graded series of ethanol then infiltrated in Eponate 12 (Pella) overnight without catalyst. The next day cells were further embedded with fresh epon containing 1.5% DMP-30 (catalyst). Culture dishes were cured at 37°C for three days, and further polymerized at 60°C overnight. Cured discs were removed from the plastic dish and 3 mm circles punched out and glued to epon blanks for sectioning. Coverslips were placed cell side down onto inverted beam capsules, filled with Epon and cured overnight at 60°C. Once polymerized, coverslips were submerged into liquid nitrogen until they separated from the beam capsule and sectioned. 80 nm thin compression free sections were obtained with a Diatome diamond knife (35 degree). Sections were picked up onto 1x2 mm formvar coated copper slot grids (Polysciences), and further stained with uranyl acetate followed by lead citrate. Grids were examined on a Hitachi H-7600 TEM operating at 80 Kv. Images were digitally captured with an XR-50, 5 megapixel CCD camera (AMT).

2.13 DGKθ truncation mutants.

Truncation mutant cloning. DGKθ truncation cDNAs were made by PCR using primers (see below) using human ^{Myc}DGKθ as a template and Q5 DNA polymerase (NEB #M0491S). GC enhancer was also included in the PCR reaction.

^{Myc}DGKθ truncation mutant	Insertion	Primers		fragment size (bp)
T1 Δ566-941	*Sal*I -- *Not*I	sense	ATC CAC TTT GCC TTT CTC TCC	1758
		antisense	CCG CAC AGC CAT GTC CTT CA	
T2 Δ262-941	*Sal*I -- *Not*I	sense	ATC CAC TTT GCC TTT CTC TCC	846
		antisense	GCT CTG CGT CTT GCT GAA	
T3 Δ1-489	*Sal*I -- *Not*I	sense	GG CAG AGA GCA GGG ATG TAG	1362
		antisense	CCC GAT CGA TCC AGA CAT GAT AAG	
T4 Δ1-255	*Sal*I --*BsrG*I	sense	CT TCA GCA AGA CGC AGA G	979
		antisense	AGC TTC GCG TGC AGC AGG TC	
T5 Δ1-580	*Sal*I -- *Not*I	sense	GA AGC TGC CCC CAG ACA GC	1089
		antisense	CCC GAT CGA TCC AGA CAT GAT AAG	
T6 Δ1-25	*Sal*I -- *Afe*I	sense	CA GCC CCG TGC TGG GCT CA	837
		antisense	ATC AAA GAT CTT CAG CGT TTG	

PCR conditions: 98°C, 5min; (98°C, 45sec; 65°C, 30sec; 72°C, 2min) x 30 cycles; 72°C, 10min. Resulting cDNAs were subcloned in frame into pRK5-Myc between *Sal*I and *Not*I (T1, T2, T3, and T5) or *Sal*I and *BsrG*I (T4) or *Sal*I and *Afe*I (T6) restriction sites. All constructs were verified by restriction enzyme digest and DNA sequencing.

Expression and DGK activity validation of DGKθ truncation constructs

HEK 293 cells were seeded in 6W dishes (1.8e6 cells/well) in opti-MEM and transfected using PEI (4 μg PEI: 1 μg plasmid DNA). 4 μg PEI was diluted into 100 μL opti-MEM and incubated for ~5m. 100 μL PEI solution was added to 100 μL of opti-MEM containing 2 μg of WT or mutant DGKθ and 0.5 μg pSuper-Venus (cell fill), and allowed to incubate for 20m at room temperature. 200 μLPEI/DNA complexes were added dropwise onto cells and incubated for ~4-5h before media was replaced with DMEM supplemented with 5%FBS. 3 days after transfection, cells were harvested in lysis buffer (25mM Tris-HCl, 100mM NaCl, 2mM EDTA, 2mM EGTA, 1%Tx-100, pH 7.4) and diluted to 1 μg/μL with SDS-sample buffer for western blot analysis (15 μg lysate per sample) or diluted to 1.5 μg/μL in lysis buffer and stored in -80°C until assayed for DGK activity. 15 μg of cell lysate was analyzed by western blot analysis and 5 μg of lysate was used for DGK activity assays.

Neuron expression and activity validation. Primary rat cortical neurons were electroporated with 2 μg of WT or mutant DGKθ and 2 μg pCAG-mCherry (cell fill) on DIV0 using a Nucleofection apparatus (Amaxa) with a rat neuron nucleofection kit (Lonza) according to the manufacturer's instructions. Cells were harvested DIV 19 with lysis buffer and diluted as described above (HEK cells) for western blot analysis and DGK activity assays. For localization experiments, rat hippocampal neurons were transfected DIV 19 with 0.5 μg WT or mutant DGKθ, 0.5 μg pCAG-mCherry, and 1 μg sypHy. 2d later, cells were fixed and stained as described above.

Electrophysiology

Hippocampal slices were prepared from DGKθ WT and KO mice ranging from 5-6 weeks in age. Field excitatory postsynaptic potentials (fEPSPs) were evoked at 50 Hz and 2 Hz with a 125 μm platinum/ iridium concentric bipolar electrode (FHC, Bowdoinham, ME) placed in the middle of stratum radiatum of CA1. A 1–2MΩ glass recording electrode filled with ACSF was positioned ~200 μm away (orthodromic) from the stimulating electrode. Recording ACSF and temperature were identical, with a flow rate of ~3mL/min. Input-output curves were obtained for each slice and responses were set to 15-20% max for experiments with picrotoxin and ~40% max for experiments without picrotoxin. 100 μm AP5 was included in the ACSF for experiments. When slices were recorded in picrotoxin, 100 μm picrotoxin was also added. For the high-frequency train, slices were stimulated at with a train of 900 stimuli at 50 Hz. At the end of the train, slices were subjected to a 2 Hz train and then 0.5 Hz train. A custom-made MatLab program was just to extract the maximum amplitude and slope for each fEPSP during the 50 Hz train and recovery. We confirmed some of these values by performing individual analysis of responses in ClampFit. For fEPSPs data, experiments are presented amplitudes of individual responses normalized to the first response of the 50 Hz train.

Data analysis and statistics

All plasticity experiments are presented as responses normalized to the average of the 20min baseline. 2min averages are presented in graphs for clarity. Representative traces in Figure 6.6 are from one DGKθ WT and KO slice with PPF values within 0.1 of the average value. Experiments. All error bars represent standard error of the mean.

CHAPTER 3.

CHARACTERIZATION OF THE EXPRESSION AND LOCALIZATION DGKΘ IN THE BRAIN

3.1 DGKθ expression is coincident with synaptogenesis

DGKθ expression has been detected in multiple regions of the late embryonic (*42*) and adult mouse brain (*22*, *43*), albeit at low cellular and temporal resolution. To date, however, there are only a few reports of cellular functions for this isoform in the literature (*38*, *44-46*), and none regarding its function in the mammalian brain. In an effort to understand the role of DGKθ in brain function, we examined DGKθ expression across multiple brain regions from adult mice. Whole-cell extracts prepared from isolated brain regions were examined by western blot analysis using an isoform-specific antibody that recognizes the c-terminal region of DGKθ protein. DGKθ was detected in all brain regions examined, including the cortex and hippocampus (**Figure 3.1A**), consistent with the previously reported mRNA expression pattern (*43*). To determine whether DGKθ is expressed in neurons or astrocytes, we compared DGKθ expression between forebrain cell extracts and primary cultures of glia from the same brain region. DGKθ was detected in the forebrain, but not in the cultured glial cells (**Figure 3.1B),** indicating that DGKθ is expressed in neuronal cells in the forebrain.

Next we examined DGKθ expression during development. Brain tissue was isolated from mice between postnatal-day 0 (P0) to 25 (P25) and subjected to western blotting. DGKθ signal intensity increased 1.8-fold from P5 to P14, and coincided with the expression of synaptophysin, an integral SV protein with an established function at synapses **(Figure 3.1C)**. A similar increase in DGKθ protein during synapse formation and development was also observed in cultured neurons (DIV 7-14, data not shown).

Figure 3.1

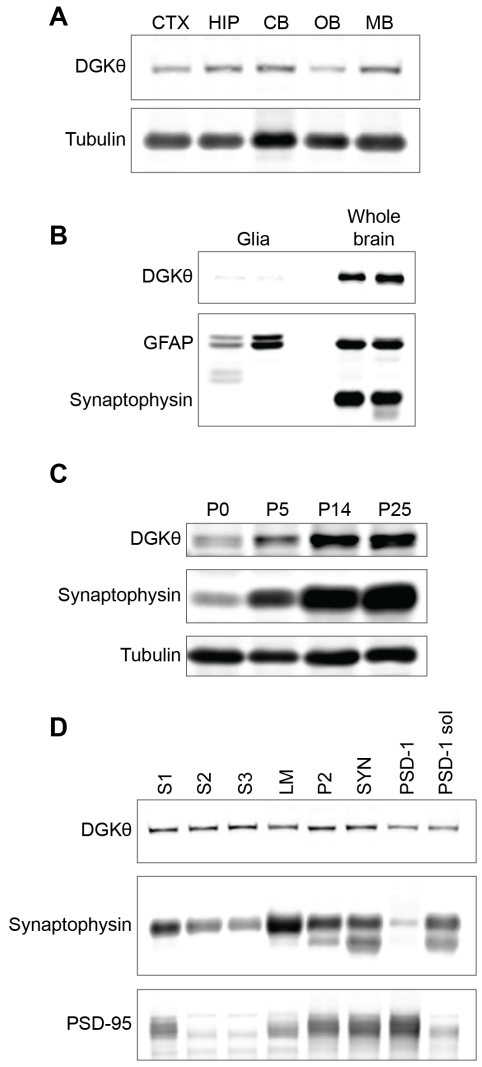

Figure 3.1 DGKθ expression is coincident with synaptogenesis. (A) Whole-cell extracts prepared from adult mouse cortex (CTX), hippocampus (HIP), cerebellum (CB), olfactory bulb (OB), midbrain (MB) were assayed for DGKθ protein expression by western blot using α-DGKθ; α-tubulin was used as a loading control. (B) Whole-cell extracts from primary glial cultures and rat whole brain were assayed for DGKθ protein expression by western blot analysis using α-DGKθ; α-GFAP (glial marker); and α-synaptophysin (neuronal marker). (C) Whole brain lysates from mice between postnatal day 0 (P0) and 25 (P25) were assayed for DGKθ protein expression by western blot using α-DGKθ; α-synaptophysin, a presynaptic protein, is shown for comparison; α-tubulin was used as a loading control. (D) Biochemical fractionation of adult mouse brain reveals DGKθ is distributed in various subcellular compartments. α-synaptophysin and α-PSD-95 (pre- and postsynaptic proteins, respectively) are shown for comparison and were used as controls for successful isolation of synaptic fractions. Post-nuclear supernatant (S1), cytosol after P2 precipitation (S2), cytosol after LM precipitation (S3), light membranes (LM), crude synaptosomes/membranes (P2), synaptosomes (SYN), postsynaptic density (PSD-I), remaining soluble fraction after PSD-I precipitation (PSD-I sol). 20 μg of protein were loaded from each fraction.

3.2 DGKθ localizes to excitatory synapses in the mouse forebrain

The onset of DGKθ protein expression during synaptogenesis suggested that DGKθ might participate in the regulation of synaptic function. To address this, subcellular fractions were prepared from adult mouse whole brain and subjected to western blot analysis. Similar amounts of DGKθ were detected in cytosolic (S1, S2, S3), microsomal (LM), and synaptosomal (P2, SYN) fractions, indicating a general distribution among subcellular compartments within the brain (**Figure 3.1D**). Furthermore, DGKθ was detected in both the synaptosome and PSD-1 fractions, suggesting its presence at both pre- and postsynaptic sites.

To verify the biochemical results we examined endogenous DGKθ localization by immunofluorescence microscopy. Neurons were co-labeled with antibodies against MAP2 and vGlut1 to illuminate dendrites and excitatory synapses, respectively. Consistent with fractionation experiments DGKθ, was detected throughout the neuron, including the cell soma, MAP2-positive dendrites, and MAP2-negative axons (**Figure 3.2A and 3.2B).** Strikingly we found that DGKθ had a punctate distribution along dendrites that significantly overlaps with the excitatory presynaptic protein vGlut1 (**Figures 3.2A and 3.2B)**. When we quantified the overlap between these two signals, we found that 62.6±1.4% of DGKθ overlapped with vGlut1 and 56.6±1.5% of vGlut1 overlapped with DGKθ per μm of dendrite (**Figure 3.2C)**.

To determine whether DGKθ is also present at inhibitory synapses, we measured the signal overlap between DGKθ and VGAT, a marker of inhibitory synapses, on MAP2-positive processes. Only 10.0±0.7% of DGKθ overlapped with VGAT per μm of

dendrite (**Figures 3.2C-3.2C**), suggesting that DGKθ preferentially localizes to excitatory synapses.

Figure 3.2

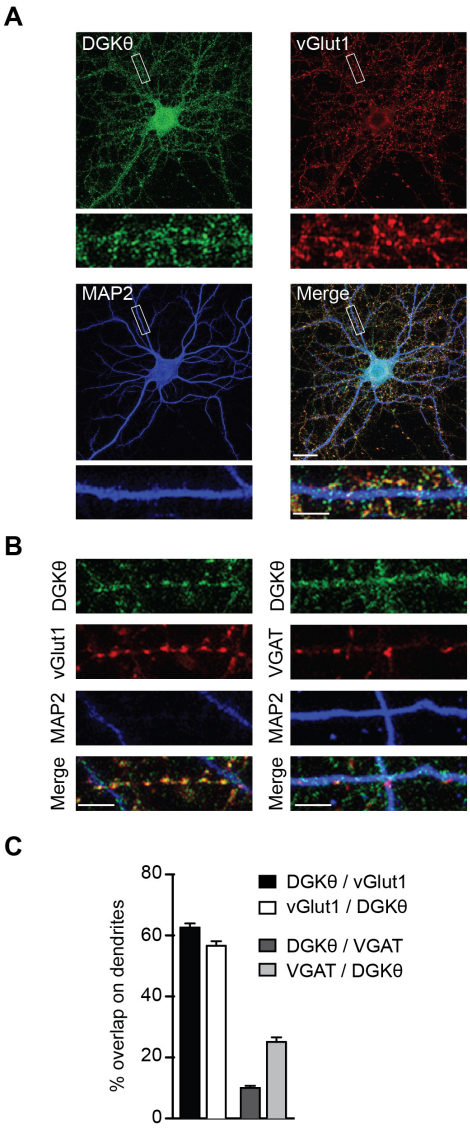

Figure 3.2. DGKθ localizes to excitatory synapses. (A-B) Cultured hippocampal neurons (DIV 28) were stained with α-DGKθ, α-vGlut1 (excitatory presynaptic protein) or α-VGAT (inhibitory synaptic marker) and MAP2 (dendritic protein). Scale bar, 20μm and 5μm (crop region). (C) Quantification of the overlap between α-DGKθ and α-vGlut1 and α-DGKθ and α-VGAT on secondary dendrites identified by MAP2 staining (MAP2-positive processes). Averages from a minimum of 3 coverslips (>3 regions per coverslip) per staining condition are shown, error bars represent SEM.

3.2 Determination of murine DGKθ half-life (*47*)

Our first step toward investigating the cellular function(s) of DGKθ in the mammalian CNS was to develop a model system where we could manipulate DGKθ protein expression using short-hairpin RNAs (shRNA). This provided a suitable background perform loss-of-function analysis as well as for evaluating mutant forms of this DGKθ. shRNAs knockdown protein expression by targeting the mRNA for degradation. Therefore, to successfully perform loss of function analysis, it is necessary to determine the protein half-life, to know how long after depletion of mRNA it takes for the protein to be degraded. To address this, cyclohexamide (CHX) was used to block all new protein synthesis in two different cell lines derived from either mouse embryonic fibroblasts (3T3) or adult neuroblasts (Neuro-2a, N2a). Samples were collected at various time-points following treatment with CHX and the abundance of DGKθ protein in whole-cell lysates was quantified by western blotting. We find that the enzyme exhibits a mean half-life of approximately 5.1 ± 2.2 h in cultured cells **(Figure 3.3).** This is consistent with the reported mean half-life of cellular proteins(*48*).

Figure 3.3

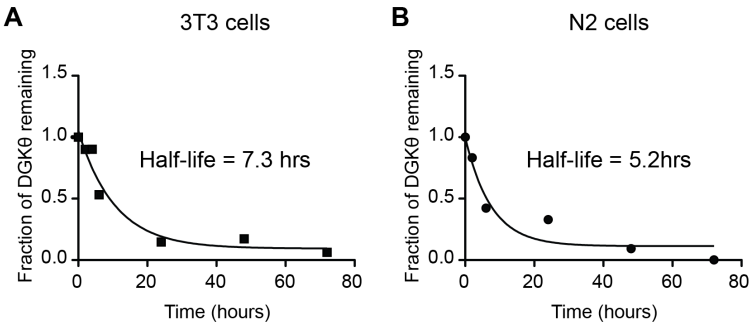

Figure 3.3. Half-life determination of murine DGKθ. 3T3 (A) and N2a (B) cells were treated with cyclohexamide (20 mg/mL) to block protein synthesis for 0, 2, 4, 6, 24, 48, and 72 h. To quantify the amount of endogenous DGKθ protein remaining in each sample over the time course, whole-cell lysates were analyzed by western blot analysis (Odyssey infrared systems, LiCor Biosciences) with α-DGKθ and α-GAPDH, a loading control. α-DGKθ signal intensity in each sample was normalized to α-GAPDH signal intensity, and then normalized to the 0 h time point for curve fitting and half-life determination.

CHAPTER 4.

shRNA-MEDIATED KNOCKDOWN OF DGKΘ ALTERS EFFICIENT RECYCLING OF SYNAPTIC VESICLES

DGKθ localization to excitatory synapses suggested a potential role for this enzyme in excitatory synaptic transmission. We predicted that reduction of DGKθ protein expression would be sufficient to alter synaptic function. To test this, we generated a short-hairpin RNA construct directed against endogenous DGKθ mRNA (**Figure 4.1A**) to suppress DGKθ protein expression. Western blot analysis showed that lentiviral-mediated expression of DGKθ-shRNA in cortical neurons resulted in >90% suppression of DGKθ protein compared to control shRNA-infected cells (**Figure 4.1A**).

4.1 Knockdown of DGKθ attenuates glutamate

Since the original study of DGK-1 in *C. elegans,* many groups have speculated that mammalian DGKs may also be involved in the regulation neurotransmitter release from synapses within the CNS (*22*, *37*). Our data showing that DGKθ is present at excitatory synapses led us to speculate that DGKθ may regulate the release of glutamate, the major excitatory neurotransmitter, from cortical neurons. We hypothesized that depletion of DGKθ protein from neurons would phenocopy loss of function mutations in DGK-1, and accelerate glutamate release. To test this, neurons expressing DGKθ-shRNA or a control shRNA were stimulated by high potassium (K^+)-induced depolarization. The concentration of glutamate released into the extracellular buffer was assayed at various time points during the 1 minute stimulation. Consistent with our original hypothesis, we observed DGKθ-depleted neurons showed elevated glutamate levels after 10 seconds of stimulation when compared to controls **(Figure 4.1B).** Surprisingly, after either 20 or 60 seconds of stimulation, DGKθ-depleted neurons released less glutamate when compared to controls at both time points.

Figure 4.1

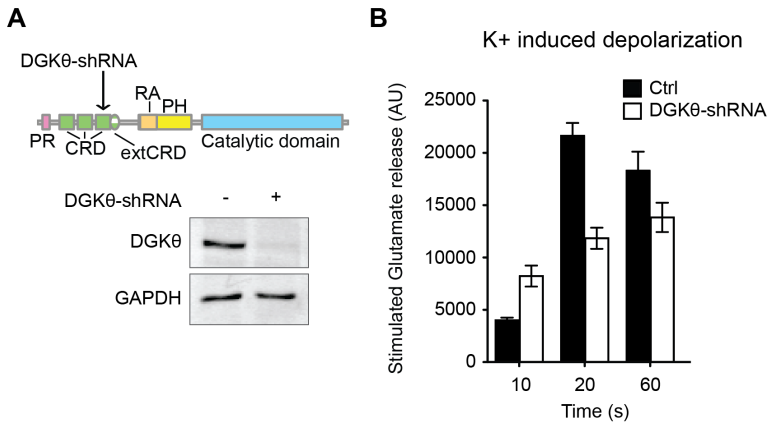

Figure 4.1. shRNA-knockdown of DGKθ attenuates glutamate release from cortical neurons. (A) Top, schematic of DGKθ protein showing the location of the DGKθ-shRNA target relative to the protein domain structure. Bottom, western blot of whole-cell lysates from rat cortical neurons expressing either control (Ctrl) or DGKθ-shRNA. α-GAPDH was used as a loading control. (B) Neurons expressing either control (Ctrl) or DGKθ-shRNAs were stimulated with 90mM KCl for 60 s. Samples collected from the extracellular media at 10-, 20-, and 60-s during stimulation were assayed to determine the concentration of glutamate released using the Amplex Red glutamate assay (see Chapter 2.7 for details).

4.2 Knockdown of DGKθ slows the rate of synaptic vesicle recycling

To determine the effect of reduced DGKθ protein levels on presynaptic function, we used the pH-sensitive optical reporter synaptophysin-pHluorin (sypHy, **Figure 4.2A** (*49*)) to monitor SV recycling dynamics. At rest, the fluorescence of sypHy is quenched by the low pH inside the SV. Upon depolarization of the nerve terminal, fusion of the SV with the membrane exposes the vesicle lumen to the neutral pH of the medium, causing a rapid increase in sypHy fluorescence. This is followed by a slow decay of the fluorescent signal as the fused vesicles undergo endocytosis and rapid reacidification. Because SV endocytosis is rate-limiting in this process (*50*), the average time constant (τ_{endo}) of the post-stimulus decay can be mainly attributed to endocytosis. To determine if acute loss of DGKθ was sufficient to alter presynaptic function, cortical neurons were co-transfected with sypHy and DGKθ-shRNA or a control shRNA, and allowed to express for 48 hours prior to measuring SV recycling kinetics. Knockdown of DGKθ produced significantly slower reuptake of sypHy or larger τ_{endo} values following high potassium (K^+)-induced depolarization compared to control neurons (**Figures 4.2B-4.2C,** τ = 59.2 ± 4.2 s and 32.4 ± 1.9 s, respectively). Moreover, expression of shRNA-resistant human DGKθ (^{myc}DGKθ) was sufficient to rescue the observed defect in endocytosis in neurons expressing DGKθ-shRNA, thus verifying the specificity of DGKθ-shRNA for the endogenous enzyme as well as the requirement for DGKθ in SV recycling **(Figures 4.2B-4.2C).**

Because K^+-depolarization is a robust and artificial stimulus, it was important to determine whether the observed defect in SV recycling also occurred in response to a more physiologic stimulus. To address this, SV recycling kinetics were measured in

control and DGKθ-shRNA expressing neurons following electrical field stimulation at 10 Hz. Consistent with K^+-induced depolarization, the average τ_{endo} values measured following a 30 s stimulation at this frequency (**Figures 4.2C-4.2E**) were significantly slower in DGKθ shRNA expressing neurons compared to controls ($\tau = 57.0 \pm 2.0$ s and $\tau = 28.4 \pm 0.9$ s, respectively). Slower SV recycling kinetics were also observed in DGKθ-knockdown neurons following a shorter (12 s) stimulation at 50 Hz **(Figures 4.3A).** In all cases, expression of ^{myc}DGKθ was able to recover the defect in SV endocytosis kinetics (**Figures 4.2B-4.2E, 4.3A-4.3B**). Taken together, these data show that DGKθ is required acutely and cell autonomously to mediate the efficient recycling of SVs following neuronal stimulation.

Figure 4.2

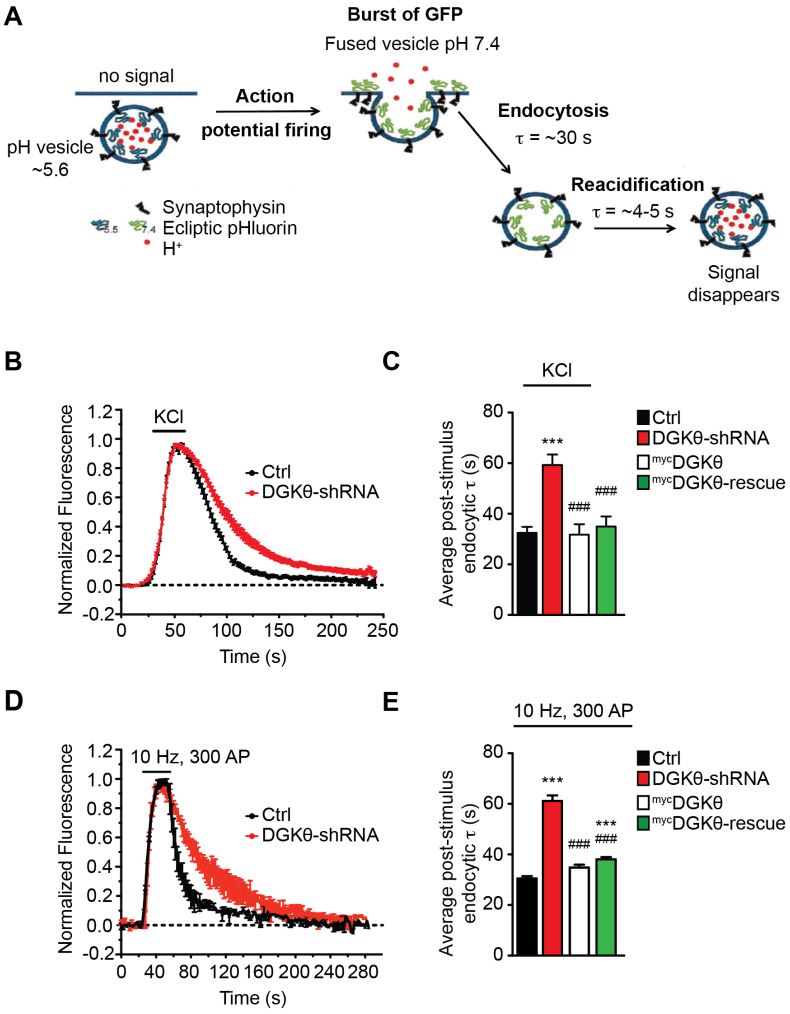
A
Burst of GFP
Fused vesicle pH 7.4
no signal
Action
potential firing
Endocytosis
τ = ~30 s
pH vesicle
~5.6
Reacidification
τ = ~4-5 s
Synaptophysin
Ecliptic pHluorin
H+
Signal
disappears
B
KCl
Normalized Fluorescence
Ctrl
DGKθ-shRNA
Time (s)
C
KCl
Average post-stimulus endocytic τ (s)
Ctrl
DGKθ-shRNA
mycDGKθ
mycDGKθ-rescue
***
###
D
10 Hz, 300 AP
Normalized Fluorescence
Ctrl
DGKθ-shRNA
Time (s)
E
10 Hz, 300 AP
Average post-stimulus endocytic τ (s)
Ctrl
DGKθ-shRNA
mycDGKθ
mycDGKθ-rescue
***
###

Figure 4.2. DGKθ regulates the kinetics of SV recycling in cortical neurons. (A) Schematic representation of the optical reporter of SV recycling dynamics, synaptophysin-pHluorin (sypHy, modified from(*49*, *51*). SypHy is composed of a pH-sensitive GFP (pKa ~ 7.1) fused to the second intravesicular loop of synaptophysin, a resident SV protein. At rest, sypHy fluorescence is quenched by the acidic pH inside the vesicle (pH~5.6). Action potential firing stimulates SV exocytosis, which exposes the vesicle lumen to the neutral extracellular external solution (pH 7.4), resulting in a rapid "burst" of fluorescence. The sypHy signal then slowly decays as to baseline as the SVs are retrieved from the plasma membrane and reacidified. The rate of endocytosis is calculated at individual boutons from the rate of fluorescence decay after stimulation. (B) Normalized average traces from rat cortical neurons expressing sypHy in response to 1 min stimulation with high K^+ buffer. Example traces for control and DGKθ-shRNA are shown in black and red, respectively. (C) Comparison of average post-stimulus endocytic time constants (τ) between control, DGKθ-shRNA, ^{myc}DGKθ (+ctrl shRNA, grey), and ^{myc}DGKθ-rescue (green) neurons. The decay phases of the normalized traces were fitted with single exponential functions and the τ values were calculated from the fits. Averages in (B-C) are from ≥6 coverslips, ≥100 boutons per condition. (D) Example normalized average traces from mouse cortical neurons expressing sypHy with control or DGKθ-shRNA (black and red, respectively) in response to a 30 s stimulation at 10 Hz. (E) Comparison of average endocytic τ values between control, DGKθ-shRNA, ^{myc}DGKθ and ^{myc}DGKθ-rescue (green) neurons in response to 300 stimuli at 10 Hz (from D). Averages in (D-E) are from ≥3 coverslips, >100 boutons per condition. For all experiments shown in Figure 4.2, data represent mean ± SEM; *** $P<0.001$ against Ctrl; ### $P<0.001$ against DGKθ-shRNA, a one-way analysis of variance (ANOVA) with Tukey's *post hoc* test. The τ values for ^{myc}DGKθ and ^{myc}DGKθ-rescue and Ctrl and ^{myc}DGKθ in (C) and (E) were not significantly different.

Figure 4.3

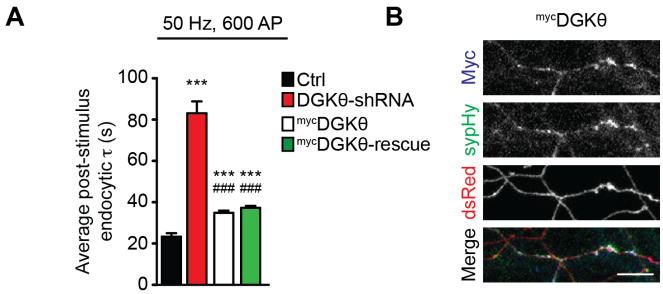

Figure 4.3. Recycling defect is rescued at synapses by ^{myc}DGKθ. (A) Average post-stimulus endocytic time constants are shown for control (Ctrl, black), DGKθ-shRNA (red), ^{myc}DGKθ (+ctrl shRNA, white) and ^{myc}DGKθ-rescue (+DGKθ-shRNA, green) neurons following a 600 stimuli at 50 Hz. Data represent mean ± SEM; *** P<0.001 against Ctrl; ### P<0.001 against DGKθ-shRNA, a one-way analysis of variance (ANOVA) with Tukey's *post hoc* test. The τ values for ^{myc}DGKθ and ^{myc}DGKθ-rescue were not significantly different. (B) Immunostaining of unstimulated ^{myc}DGKθ expressing neurons from (A) with α-GFP (sypHy, green) and α-Myc (^{myc}DGKθ, blue) antibodies shows significant overlap between the two signals along neuronal processes. ^{myc}DGKθ colocalization with sypHy indicates ^{myc}DGKθ rescues defective SV recycling in DGKθ-shRNA neurons at synaptic sites.

CHAPTER 5.

DGKΘ KNOCK-OUT MICE SHOW DEFECTS IN SYNAPTIC VESICLE CYCLING AT CENTRAL SYNAPSES

5.1 DGKθ knock-out mice have reduced synaptic DGK activity

Since transient depletion of DGKθ was sufficient to alter presynaptic function, we wondered if loss of DGKθ during neuronal development would produce a similar phenotype. To address this, we generated a conventional DGKθ homozygous knock-out (KO) mouse from heterozygous $Dgkq^{tm1a(KOMP)Wtsi}$ (Het) animals (see methods, **Figure 5.1A**). The genotypes of wild-type (WT), Het, and KO mice were confirmed by conventional PCR with primers targeting the KO allele and by western blot (**Figures 5.1A and 5.1B**). DGKθ KO mice appeared overtly healthy and did not display any obvious gross morphology difference compared to WT mice (body size, mating, lifespan, data not shown). With eight additional DGK isoforms expressed in neuronal tissue, we considered the possibility that another DGK isoform may compensate for synaptic defects produced by the loss of DGKθ. To address this, we probed whole-cell extracts prepared from WT and KO brain tissue antibodies specific for other neuronal DGK isoforms. Again, no significant difference in signal intensity was detected between WT and KO samples for any of the DGKs examined (-δ, -γ, -ι, and -ζ, **Figure 5.1C**). Thus, it is unlikely that another neuronal DGK isoform is compensating for loss of DGKθ.

Since all DGK isoforms catalyze the same reaction, phosphorylation of DAG to produce PtdOH, another potential mechanism for compensation by other DGKs is through their catalytic activity. We measured total DGK activity in cell extracts prepared from adult WT and KO forebrain tissue using an *in vitro* assay has been is used to measure activity of purified forms of DGKθ, DGKζ, and DGKδ ((*41*) and unpublished data). Calcium was excluded from the DGK assay buffer to minimized activity from type

I DGKs (α, β, γ). Interestingly, loss of DGKθ produced significant decrease in DGK activity measured in KO tissue compared WT (**Figure 5.1D**).

Figure 5.1

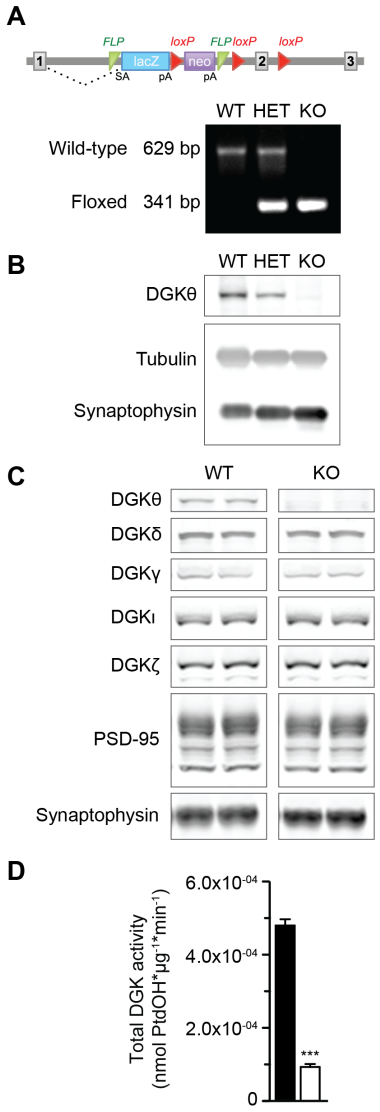

Figure 5.1. Total DGK activity is reduced in DGKθ KO mice. (A) Top, schematic of DGKθ knock-out mouse allele, Dgkq$^{tm1a(KOMP)Wtsi}$(*52*). Exon 1 is spliced to the artificial splice acceptor (SA) in front of lacZ instead of another exon in the DGKθ gene. The poly-adenylation site (pA) terminates transcription after lacZ, preventing the transcription of the DGKθ RNA. Bottom, typical result of PCR for genotyping. Bands at 629bp and 341bp are indicative of wild-type (WT) and DGKθ KO alleles, respectively. (B) Western blot analysis of whole-cell lysates prepared from brain tissue from 5 week-old WT, DGKθ heterozygous and KO littermates. α-tubulin was used as a loading control, α-synaptophysin were used as a marker for brain tissue. (C) Western blot analysis of brain tissue isolated from 2 pairs of WT and DGKθ KO mice, run on the same gel. Samples were immunoblotted with antibodies against DGKθ, -γ, -ι, -ζ, representing 4 classes of DGKs. α-synaptophysin and α-PSD95 are shown for comparison as controls. (D) Average total DGK activity measured in 5 µg of S1 cytosolic fractions from 5 pairs of age-matched WT and DGKθ KO forebrain tissues (age range from 2 weeks - 6 months). Averages include 3 technical replicates per sample, N = 15 (5, 5). Error bars = ± SEM. Student's t test, *** P<0.0001 against WT.

5.2 DGKθ catalytic activity is required for kinetically efficient SV recycling

Because developmental loss of DGKθ produced a significant reduction in DGK activity that was not compensated for by other DGKs, we predicted that DGKθ KO neurons might exhibit defects in SV recycling similar to those observed in DGKθ-shRNA expressing cells **(Figure 4)**. To address this, neurons derived from WT and DGKθ KO mice were transiently transfected with sypHy and post-stimulus recovery rates following a 50Hz, 600AP stimulus were determined **(Figure 5.2A).** Consistent with the slower τ_{endo} values measured in DGKθ-knockdown neurons, we found that DGKθ KO neurons also showed significantly larger τ_{endo} compared to WT neurons (KO $\tau_{endo} = 63.4 \pm 1.3$ s vs. WT $\tau_{endo} = 23.0 \pm 0.8$ s) that could be recovered by expression of ^{Myc}DGKθ (**Figure 5.2A-5.2B**). Due to the significant reduction of total DGK activity in DGKθ KO tissue, we predicted that the catalytic activity of DGKθ might be necessary for it to promote efficient recycling of SVs. Previous work has shown that DGKθ catalytic activity can be completely abolished by a single point mutation (G648A) in the conserved ATP binding site within the catalytic domain of the enzyme (*39*). We tested the ability of this kinase-dead mutant of DGKθ (^{Myc}DGKθ-kd) to rescue the defect in SV recycling observed in DGKθ KO neurons. Consistent with our hypothesis, expression of ^{Myc}DGKθ-kd in KO neurons was unable to recover the delay in SV recycling kinetics (**Figure 5.2B**). We confirmed that ^{Myc}DGKθ and ^{Myc}DGKθ-kd were expressed at similar levels in neurons and HEK cells as well as validated the expected DGK activities for both recombinant proteins (**Figures 5.2C-5.2D,** and data not shown). Furthermore, when KO neurons expressing ^{Myc}DGKθ-kd with sypHy were labeled with antibodies against the epitope tags (anti-myc and anti-GFP, respectively), we observed significant overlap between the two

signals along neuronal processes (**Figure 5.2E**). The synaptic localization of ^{Myc}DGKθ-kd argues that this mutant fails to rescue the SV recycling defect in KO neurons due to its loss of catalytic activity, and not mis-targeting of the protein. Taken together, these data demonstrate that DGKθ catalytic activity is necessary for efficient recycling of SVs following sustained stimulation.

Figure 5.2

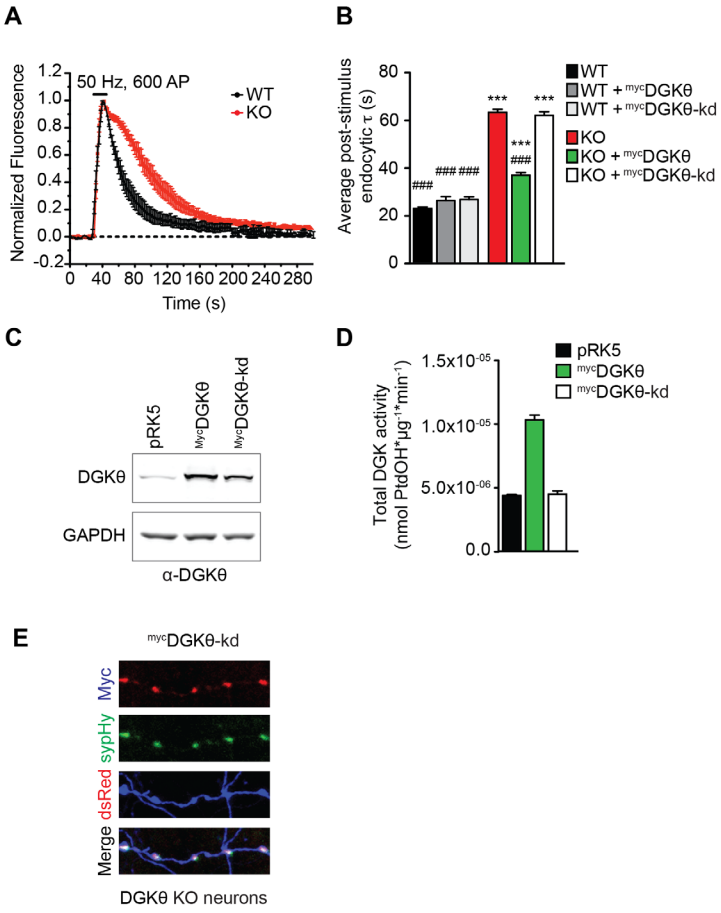

Figure 5.2. DGKθ activity regulates SV recycling kinetics *in vivo*. (A) Normalized average traces from wild-type (WT, black) and DGKθ KO (red) neurons expressing sypHy in response to 600 stimuli at 50 Hz. Averages are from >5 regions per genotype, >3 coverslips, from 3 experiments (>140 ROIs). (B) Comparison of average post-stimulus (600 AP, 50 Hz) endocytic time constants between WT and DGKθ KO neurons expressing empty vector, ^{myc}DGKθ, or kinase-dead DGKθ (^{myc}DGKθ-kd). All averages in are from ≥3 batches of WT and KO neurons, ≥3 coverslips, ≥50 boutons per condition; data represent mean ± SEM; *** P< 0.001 against WT; ### P<0.001 against KO, ANOVA with Tukey's *post hoc* test. Average τ values measured in KO neurons (+empty vector) were not significantly different from KO + ^{myc}DGKθ-kd. (C-D) ^{myc}DGKθ and ^{myc}DGKθ-kd are expressed at similar levels in neurons and exhibit expected DGK activities in neuronal lysates. (C) Western blot analysis of whole-cell lysates prepared from cortical neurons (DIV 18) electroporated with pRK5, ^{myc}DGKθ, or ^{myc}DGKθ-kd. α-DGKθ mAb was used to compare endogenous DGKθ expression in pRK5 expressing neurons with ^{myc}DGKθ and ^{myc}DGKθ-kd. α-GAPDH was used as a loading control. 5 µg of total protein from each lysate analyzed in (C) were also assayed for total DGK activity (D) using an *in vitro* assay (for details see Chapter 2.11). Overexpression of ^{myc}DGKθ, but not ^{myc}DGKθ-kd, produced a significant increase in DGK activity compared to control (pRK5) neurons. (E) DGKθ KO neurons (DIV 20) expressing sypHy, mCherry, ^{myc}DGKθ-kd were stained with α-myc (red), GFP (green), and α-dsRED (blue), merge panel (bottom). Together, data shown in (C-D) demonstrate that the failure of ^{myc}DGKθ-kd to rescue SV recycling kinetics in DGKθ KO neurons is due to its lack of catalytic activity, and not altered expression level or subcellular targeting.

It is well known that the strength of the stimulus can activate distinct recycling mechanisms (*16*, *53*). To determine if DGKθ is required for kinetically efficient SV recycling following elevated and mild neuronal activity, we evaluated the effect of the stimulation frequency and duration of stimulation on τ_{endo} in WT and KO neurons. Sustained stimulation at 10Hz and 50Hz resulted in significantly slower kinetics of SV endocytosis in KO neurons compared to WT (**Figures 5.3A-5.3C**). Interestingly, while higher frequency stimulation produced the largest change in τ_{endow} between WT and KO neurons, we found that SV recycling kinetics became more impaired with increasing number of action potentials at both frequencies (**Figures 5.3A-5.3C**). Thus, we conclude from these data during periods of sustained neuronal activity, when more action potentials are fired, DGKθ plays a more critical role in promoting efficient retrieval of SVs.

A potential consequence of reduced synaptic DGK activity found in DGKθ KO mice could be elevated levels of DAG in the plasma membrane. Since functional analogues of DAG are known to potentiate synaptic transmission (*27*), we hypothesized that the slowed recycling kinetics measured in DGKθ KO neurons could be the results of augmented SV exocytosis. To resolve the rate of SV exocytosis from the SV recycling dynamics reported by sypHy, WT and KO neurons were stimulated in the presence of the vesicular ATPase inhibitor, bafilomycin A1 (baf) (*54*). Baf blocks the reacidification of SVs without affecting recycling dynamics (*55*), thus SV exocytosis kinetics can be determined from the increase in fluorescence during neuronal stimulation. The rate of SV exocytosis measured in WT and KO neurons **(Figure 5.4)** were essentially identical**.** KO neurons did show a small increase in the maximum sypHy amplitude; however, this did

not reach statistical significance. Taken together, these data demonstrate that the SV recycling defect observed in DGKθ KO neurons is not secondary to altered exocytosis, and argues that DGKθ directly regulates the rate of SV endocytosis.

Figure 5.3

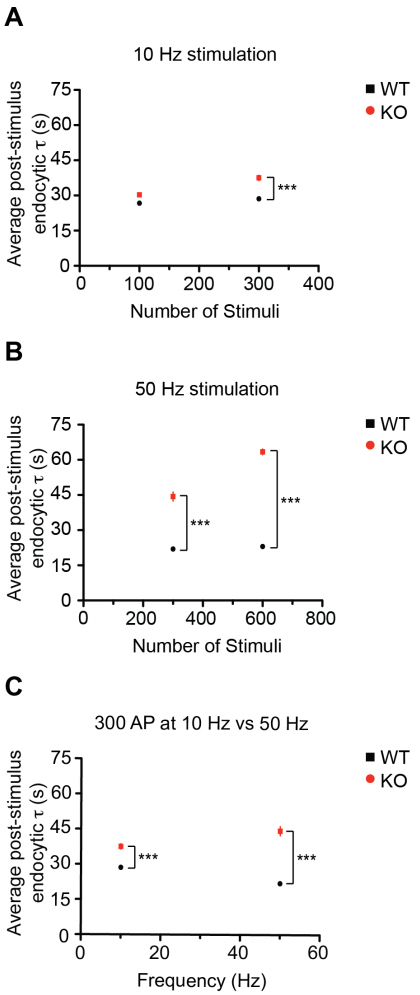

Figure 5.3. DGK0 promotes efficient recycling of SVs following elevated neuronal activity. (A) Comparison of the average endocytic time constants measured following 100 or 300 stimuli at 10 Hz. Averages are from ≥ 2 batches of WT and KO neurons, ≥3 coverslips, ≥200 boutons per condition. For experiments shown in panels (A-C), data represent mean ± SEM; *** $P < 0.001$, ANOVA with Tukey's *post hoc* test. (B) Comparison of the average endocytic time constants measured following 300 or 600 (from Figure 5.2) stimuli at 50 Hz. Averages are from ≥ 2 batches of WT and KO neurons, ≥3 coverslips, ≥120 boutons per condition. (C) Comparison of the average endocytic time constants measured following 300 stimuli at 10 Hz and 50 Hz shown in panels (A-B).

Figure 5.

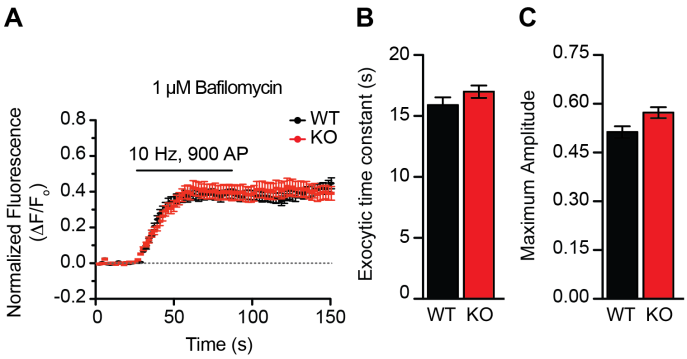

Figure 5.4. SV exocytosis kinetics are normal in DGKθ KO neurons. (A) Average traces of from WT and DGKθ KO neurons stimulated for 90 s at 10 Hz in the presence of 1 µM bafilomycin, a vesicular ATPase inhibitor. Traces were normalized to the average baseline before stimulation. Representative traces for each genotype are shown, averages shown are from one coverslip per genotype, >100 ROIs, data represent mean from ± SEM. (B) Average exocytic rate constants were determined by normalizing $\Delta F/F_0$ traces to the average maximum amplitude (average 10 frames after 90 s, 10 Hz stimulus). Tau values were calculated by fitting the rise-portion of the response during stimulation to a one-phase association curve. All averages in are from ≥ 3 batches of WT and KO neurons, ≥3 coverslips, ≥300 boutons per condition; data represent mean ± SEM. (C) Maximum amplitude of sypHy fluorescence response following a 90 s stimulation at 10 Hz. Values are calculated after normalization to baseline from $\Delta F/F_0$ curves (example of traces shown in (A). All averages in are from ≥ 3 batches of WT and KO neurons, ≥3 coverslips, ≥300 boutons per condition; data represent mean ± SEM. WT-black, KO-red.

CHAPTER 6.

INSIGHTS INTO THE MECHANISM OF DGKΘ-MEDIATED REGULATION OF SYNAPTIC VESICLE RECYCLING

Current research is focused on exploring the possible mechanism by which DGKθ catalytic activity promotes efficient recycling of SV following neuronal activity. To date, we have used three different approaches to gain insight into the mechanism (1) structure-function analysis of DGKθ, (2) ultrastructure analysis of DGKθ WT and KO synapses, and (3) electrophysiological analysis of DGKθ WT and KO hippocampal slices. While these studies are still preliminary, recent experiments have produced some interesting and promising data, which are discussed below. Ongoing and future experiments that validate these findings will undoubtedly provide valuable insight regarding the mechanism behind the synaptic function of DGKθ, PtdOH and DAG.

6.1 Structure-function analysis of DGKθ

The finding that a kinase-dead mutant of DGKθ could not rescue the defects in SV recycling in DGKθ KO neurons indicates that the catalytic activity of the DGKθ is required for its role in promoting efficient retrieval of SVs following neuronal activity. These data, together with the total DGK activity and expression analysis of other DGK isoforms **(Figure 5.1C-5.1D)** suggests that it is unlikely that another DGK isoform is compensating for the loss of DGKθ in the KO mice. Since all DGK isoforms catalyze the same reaction, we were curious if any of the other structural components predicted by the primary amino acid sequence, particularly those that distinguish DGKθ from the other nine mammalian isoforms, were involved in specifying a role for DGKθ in SV recycling.

Mammalian DGKs are classified into five subtypes based on similarities in their primary amino acid sequence (**see Chapter 1.3**). As the only type V DGK isoform, DGKθ protein structure is distinguished by the presence of three cysteine-rich domains

(CRDs, other DGK isoforms only have 2), a pleckstrin homology (PH) domain (also present in type II DGKs), a Ras-associating domain (RA) partially overlapping the PH domain, and an N-terminal proline/glycine-rich domain (PRD). To determine which structural features of DGKθ are required for its role in SV recycling, we generated a series of rationally designed DGKθ mutants that were truncated from either the N- or C-terminus **(T1-T6, Figure 6.1A).** Western blot analysis using an antibody against the N-terminal Myc-tag confirmed the expression of T1-T6 in HEK cells (**Figures 6.1B-6.1D**) and primary cortical neurons (**Figures 6.1E-6.1F, respectively**) by producing bands at the predicted molecular weights for each mutant. When the lysates were probed with a DGKθ antibody raised against an epitope containing the C-terminal region of human DGKθ (aa 691-820), all the mutants except for T1 and T2 were detected (**Figures 6.1C and 6.1E)**. These results are expected as both T1 and T2 both contain large C-terminal truncations that removed the entire catalytic domain, which contains the epitope recognized by the antibody. Collectively, these data show that truncation of DGKθ does not lead to rapid degradation in HEK cells or neurons.

Figure 6.1

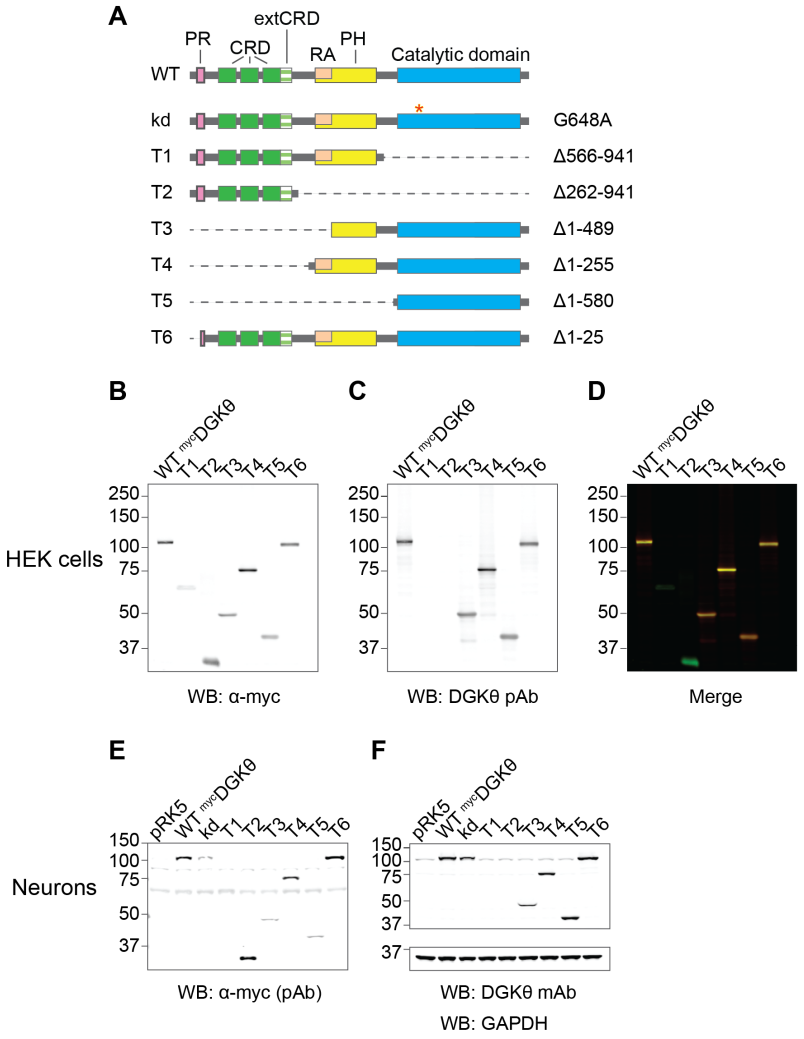

Figure 6.1. DGKθ truncation mutant proteins are stably expressed in HEK cells and primary neurons. (A) Schematic of wild-type DGKθ protein domain structure (WT) compared to the DGKθ kinase-dead mutant (kd, G648A, position shown with red *) and six truncation mutants (T1-T6). Residues deleted are shown on the right. WT and mutant DGKθ constructs were cloned into pRK5 and tagged at the N-terminus with Myc. PR, proline-rich domain; CRD, cysteine-rich domains (3 CRDs); extCRD, extended CRD; PH, pleckstrin homology domain, RA, ras-associated domain. (B-D) Western blot analysis of HEK lysates transfected with either WT or mutant DGKθ using an antibody against the epitope tag (α-Myc (B) and (D) in green) and endogenous DGKθ ((C) α- DGKθ pAb and (D) red) that recognizes an epitope in the catalytic domain of DGKθ. WT and T3-T6 were recognized by both antibodies, but T1 and T2 were only recognized by α-Myc, which is expected since the catalytic domain was removed from these two mutants. (E-F) Western blot analysis of primary cortical neurons electroporated with WT and mutant DGKθ constructs shows these proteins are also stably expressed in neurons.

Previous studies have shown that DGKθ catalytic activity is sensitive to mutation and truncation(*39*). To measure DGK catalytic activity of our truncation mutants we assayed their activity in whole-cell lysates. For these experiments, lysates prepared from HEK cells transiently transfected with either WT DGKθ (positive control), DGKθ-kd (negative control) or DGKθ truncation mutants (T1-T6) were assayed *in vitro* for total DGK activity. Consistent with previous studies, expression of all but one truncation mutant (T6) in HEK cells did not produce a significant increase in DGK activity in lysates (**Figure 6.2B**). Interestingly, overexpression of T6, the smallest truncation mutant with only 25 amino acids removed from the N-terminus, produced a significant increase in DGK activity compared to control (empty vector, pRK5), similar to that measured in lysates expressing the full-length DGK enzyme**.** Similar experiments were performed in neurons (**Figure 6.2C**). Briefly, cortical neurons expressing WT DGKθ, DGKθ-kd or T1-T6 were harvested at DIV 19, a time when endogenous DGKθ protein levels are high, and whole-cell lysates were assayed for DGK activity. While expression of DGKθ-kd or T1-T5 did not produce lysates with a significant increase in DGK activity over control (empty vector), lysates from neurons expressing WT DGKθ or T6 were significantly elevated for DGK activity **(Figure 6.2C).** Since DGKθ tends to aggregate during purification (unpublished observation), one possibility for the lack of activity is that the truncated enzyme is aggregated in cells. However, the stable expression of all the mutants in both HEK cells and neurons, as well as the uniform distribution of the mutants within the soma of neurons (see below) argues against this notion.

Figure 6.2

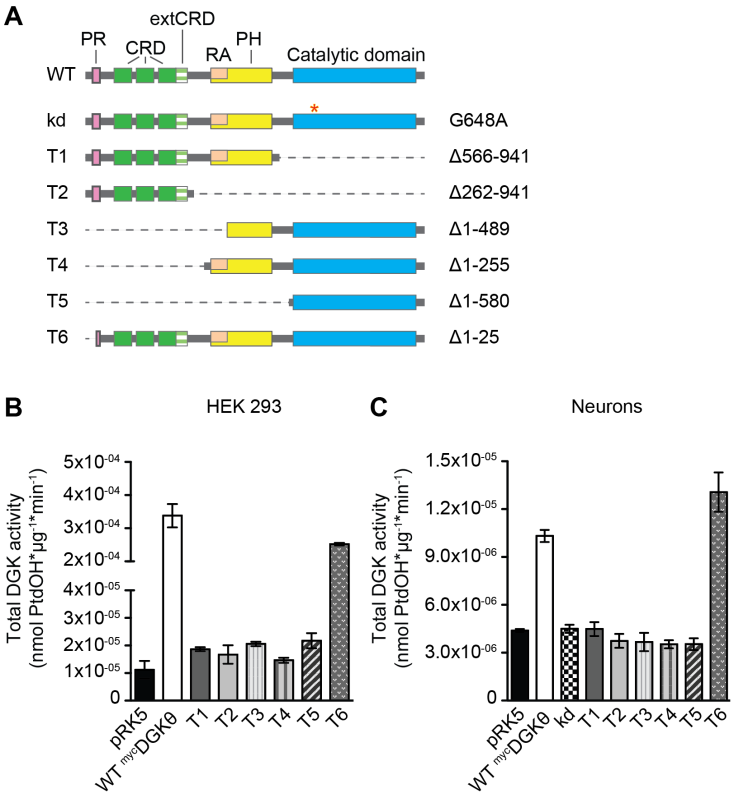

Figure 6.2. DGKθ catalytic activity is high sensitive to mutation
(A) Schematic of wild-type DGKθ protein domain structure (WT) compared to the DGKθ kinase-dead mutant (kd, G648A, position shown with red *) and six truncation mutants (T1-T6). Residues deleted are shown on the right. (B-C) Total DGK activity was assayed in HEK (B) and neuronal (C) cell lysates shown in Figure 6.1. In both cell types, there was no significant difference in DGK activity measured in lysates expressing T1-T5 or DGKθ-kd compared to control. Expression of WT DGKθ or T6 resulted in a significant increase in total DGK activity. Averages shown from 3 technical replicates per sample, N = 1 for each cell type, error bars = ± SEM.

Given our ability to express truncation mutants, we were curious to determine whether they affected DGKθ subcellular localization or neuronal morphology. For this study, , hippocampal neurons were transiently transfected with WT DGKθ, DGKθ-kd or T1-T6, along with sypHy, to identify synapses, and dsRed, to examine the cell morphology. Preliminary analysis of neurons labeled with antibodies against the Myc (DGKθ) and GFP (sypHy) epitope tags revealed significant overlap between the two signals along neuronal processes for WT DGKθ (**Figure 6.2B**) and all DGKθ mutants (**Figure 6.2C)** except T3 and T4 (**Figure 6.2D**). While these findings still need to be confirmed, they suggest that truncation of DGKθ does not significantly alter subcellular targeting of the enzyme. Of note, the cell morphology of neurons expressing the truncated WT DGKθ mutants did appear abnormal, albeit with extra branching along axons/dendrites as well as neurite-like protrusions from the neuronal processes (**Figures 6.2C-6.2D**). Future studies examining the effect of these mutants on spine development and neuronal morphology are necessary to determine and classify the mutant phenotype(s) produced as a result of their expression.

Figure 6.3

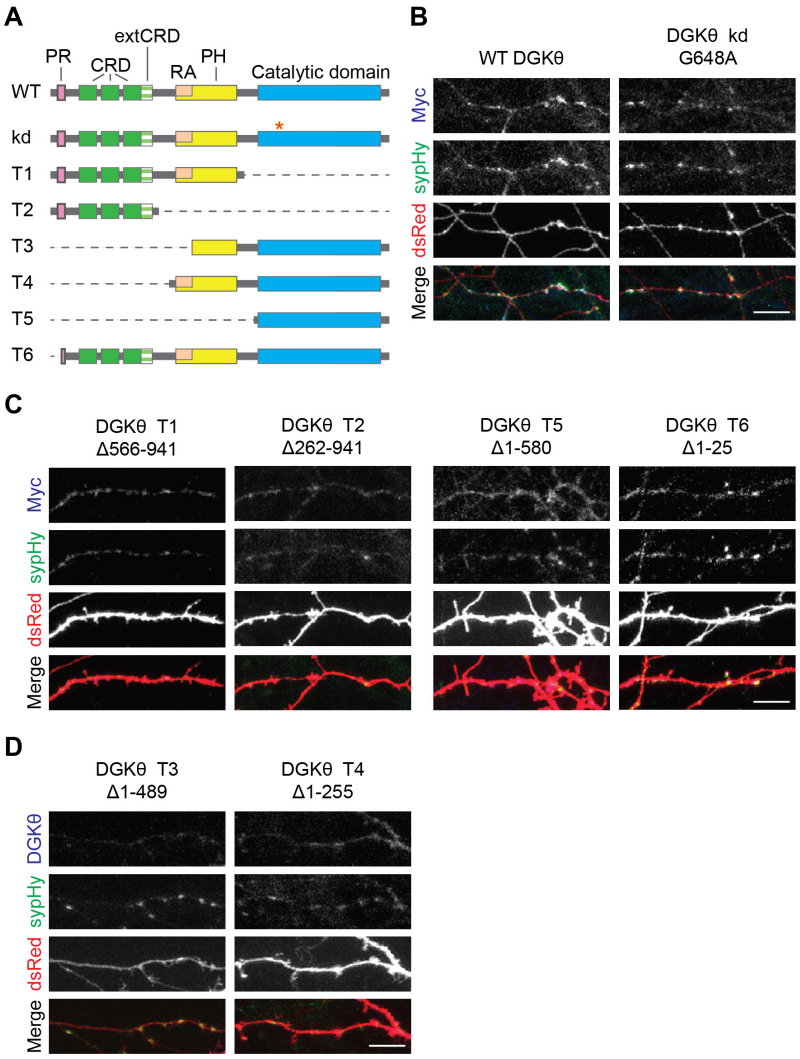

Figure 6.3. Synaptic localization of DGKθ truncation mutants
(A) Schematic of wild-type DGKθ protein domain structure (WT) compared to the DGKθ kinase-dead mutant (kd, G648A, position shown with red *) and six truncation mutants (T1-T6). Residues deleted are shown on the right. (B-D) Hippocampal neurons were transiently transfected with WT DGKθ, DGKθ-kd or T1-T6 (blue), along with sypHy (green), to identify synapses, and dsRed (red), to examine the cell morphology. (B) WT DGKθ, DGKθ-kd and (C) T1, T2, T5, and T6 localize with sypHy on axons. (D) T3 and T4 show more diffuse localization in the soma and neuronal processes, and do not show strong overlap with sypHy. More experiments are necessary to confirm and quantify these observations.

T6, the only mutant that exhibited WT DGKθ activity in both HEK cells and neurons is of particular interest as it is not only catalytically active, but the 25 amino acids that are absent from this mutant enzyme encode a putative Src-homology (SH3) domain within the N-terminal PRD (*43*). Numerous endocytic adaptor proteins, with established roles in SV recycling, are known to interact with dynamin 1 through binding of their SH3 domains with the PRD on dynamin (*56*). This is particularly interesting as dynamin 1 is abundant in neuronal tissue and known which plays an essential role in the fission reaction during clathrin-dependent and clathrin independent endocytosis of SVs (*57-59*). We therefore considered a few potential mechanisms-that are not mutually exclusive for how DGKθ is regulating the kinetics of SV endocytosis:

1) DGKθ production of PtdOH recruits (and activates) endocytic adaptor proteins and/or dynamin 1 to endocytic sites
2) DGKθ directly interacts with endocytic adaptor proteins/dynamin 1, these interactions modulate DGKθ activity, leading to changes in PtdOH production→ #1 or for regeneration of PtdIns

If endogenous DGKθ activity is regulated by an endocytic protein via binding to its N-terminus, the T6 mutant should not be able to rescue the SV defect in DGKθ KO neurons. On going experiments testing the ability of this mutant to rescue the defect in SV recycling in DGKθ KO neurons will provide important insight into the potential mechanism for how DGKθ is regulating SV recycling

6.2 Ultrastructural analysis of DGKθ KO synapses

To further investigate how the loss of DGKθ results in defective SV retrieval following neuronal activity, we used electron microscopy to perform ultrastructural

analyses of neuronal synapses from wild type or DGKθ KO mice. The high resolution of this methodology has can be used to characterize SVs within the presynaptic bouton (size, number, distance to the active zone), as well as reveal structural abnormalities (endocytic intermediates, stranded SVs, clathrin coated SVs, etc.) that could explain the defects in SV recycling in DGKθ mice (*60*, *61*). For these experiments, we first examined the synaptic structure of CA1 pyramidal synapses in the hippocampi of WT and DGKθ KO mice. There were two obvious differences in DGKθ KO synapses compared to WT. First, DGKθ KO synapses have more SVs compared to WT **(Figures 6.4A-6.4B).** While this observation appears to be inconsistent with the sypHy data that showed no difference SV pool size (**Figure 5.4),** it could be explained by the second notable difference at DGKθ KO synapses, the distribution and localization of the SVs. There is a notable difference in the number of SVs in each electron micrograph of DGKθ KO slices, however, several of these SVs were not associated with a conventional synaptic structure, presynaptic bouton opposite to postsynaptic terminal with a prominent PSD (**Figures 6.4A-6.4B).** One possible explanation for the possible redistribution of SVs could be altered DAG levels in synaptic and extra-synaptic membranes. Since DAG is known to stimulate the priming activity of Munc13-1, and DGKθ is localized to many subcellular regions, it is possible that DAG levels are elevated throughout DGKθ KO neurons, leading to the mislocalization of synaptic proteins and SVs. At some DGKθ KO synapses, we observed tethers between SVs that were not immediately adjacent to the presynaptic membrane (**Figure 6.4A-6.4B**), which could reflect an endocytic intermediate or defective SV priming.

While these results still need to be confirmed, we are encouraged by preliminary ultrastructural analysis of synapses from neuronal cultures derived from WT and DGKθ KO mice (**Figures 6.5)**. Examination of synapses from 2-3 week-old cultures of primary neurons revealed similar differences in the number and distribution of SVs in DGKθ KO neurons compared to WT (**Figures 6.5A-6.5B**). A third, less obvious, difference detected at KO synapses in cultured neurons was the presence of membrane invagination at the presynaptic plasma membrane (**Figures 6.5A-6.5B)**, which could reflect the slower reuptake of SVs during basal neurotransmission. Ongoing research in the laboratory is focused on further analysis and quantification of the differences in SV size, distribution, and membrane dynamics between WT and DGKθ KO synapses. Nevertheless, there is an obvious phenotype in DGKθ KO synapses, which has been observed now in two different pairs of WT and KO mice as well as primary cultured neurons from these animals.

Figure 6.4

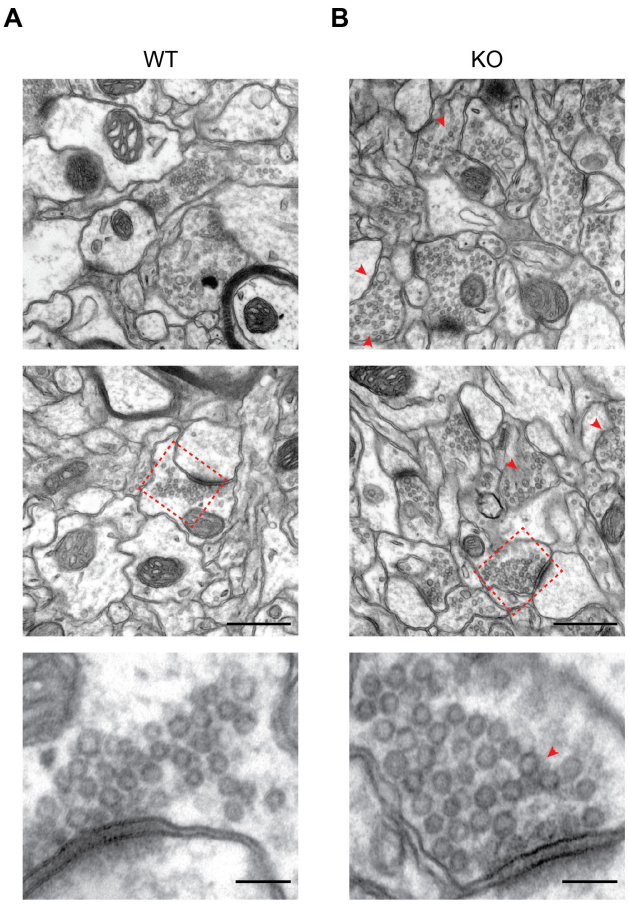

Figure 6.4. Loss of DGKθ activity produces changes in the number and localization of SVs in CA1 neurons. (A-B) Top and middle, electron micrographs of two representative synapses from neurons in the CA1 region of wild-type (WT) and DGKθ KO hippocampal sections. Ultrastructural analysis of DGKθ KO tissue showed increased number of SVs as well as clusters of SVs at non-synaptic sites (red arrows). Lower panel, higher magnification view of WT and KO synapses (red box, middle panel) reveals tethers between SVs ~100nm away from the plasma membrane at KO synapses (red arrow) but not WT synapses. SV-tethers were are a less common phenotype found in KO electron micrographs and were not observed at all KO synapses. While these data required further quantitative validation, the phenotype was observed at the majority of synapses examined (>40 for each genotype) from two different pairs of aged-matched WT and KO animals (6 mo. old). Scale bar, 500 nm. Scale bar, 100 nm.

Figure 6.5

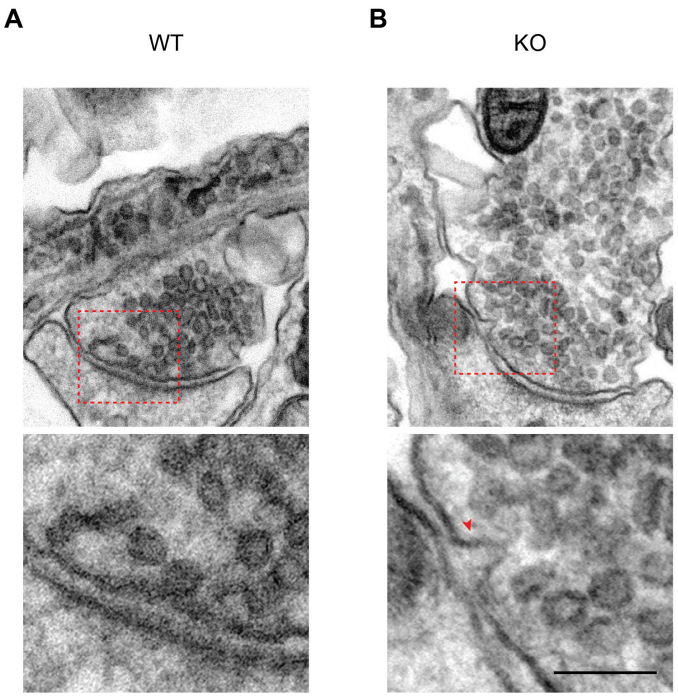

Figure 6.5. Ultrastructural changes in SV number and distribution are also observed in cultured cortical neurons derived from DGKθ KO animals. (A-B) Top panel, electron micrographs of WT and DGKθ KO synapses from primary cortical neurons (DIV 15). Ultrastructural analysis of DGKθ KO synapses from culture neurons showed a similar phenotype to that observed in CA1 neurons from hippocampal slices. Lower panel, high magnification view of KO synapses revealed membrane invaginations (red arrow, observed 3 times in KO, 1 time in WT micrographs). These data required further quantitative validation to confirm the apparent phenotype observed in KO neurons. Representative images for each genotype were selected from >40 synapses examined, from three different batches of cultured neurons (DIV 15-21). Scale bar, 100 nm.

6.3 Electrophysiological properties of DGKθ KO mice

These experiments were done in collaboration with Dr. Lenora Volk currently at the University of Texas-Southwestern, Department of Neuroscience

Since DGKθ colocalizes with vGlut1 at presynaptic glutamatergic terminals of hippocampal neurons *in vitro* and affects SV recycling (**Figures 3.2, 4.2, 5.2)**, we considered the possibility that DGKθ regulates excitatory synaptic transmission. To test this hypothesis, we examined excitatory synaptic function in WT and DGKθ KO mice by stimulating the glutamatergic terminals of CA3 neurons (Schaffer collaterals, SC), which project onto excitatory pyramidal cells and inhibitory interneurons of the CA1 area. Loss of DGKθ is predicted to produce elevated DAG levels, which has been shown to increase SV release probability(*32*, *37*) . While we did not observe any change in SV exocytosis in DGKθ KO neurons using the sypHy reporter **(Figure 5.4)**, we speculated that this assay may not be sensitive or fast enough to pick up a small change in SV release probability. Therefore, we compared paired-pulse facilitation (PPF), an established measure of basal SV release probability at SC-CA1 WT and DGKθ KO synapses. At all inter-stimulus intervals (ISI), we observed slightly increased PPF in DGKθ KO slices, compared to slices prepared from WT animals **(Figure 6.6A)**, suggesting that SV release is slightly impaired. However, these results did not achieve significance (P = 0.13, genotype effect, two-way repeated measures ANOVA; n = 14/group) and the effect of ISI did not differ between genotypes (P=0.64, interaction effect, two-way repeated measures ANOVA). More experiments are necessary to determine if this trend towards increased PPF is real, especially at shorter ISI (25-50 ms).

To test the role of DGKθ in modulating excitatory drive specifically onto excitatory neurons, we measured PPF at SC-CA1 synapses when inhibitory transmission was blocked with picrotoxin, a $GABA_A$-receptor antagonist. Interestingly, DGKθ KO synapses showed slightly decreased PPF at all ISI (**Figure 6.6B**) ($P = 0.09$, genotype effect, two-way repeated measures ANOVA; n = 10 WT, n = 11 KO). We observed the most significant difference at the smallest ISI ($P = 0.07$, interaction effect of ISI and genotype, two-way repeated measures ANOVA; $P<0.05$ at 25 ms, post hoc Bonferroni test).

Lower paired-pulse ratios (PPR) values, as we observed in the presence of picrotoxin, are usually indicative of an increased basal SV release probability. These results could suggest that excitatory drive onto excitatory neurons is slightly increased. However, PPR values measured at short ISI (25 and 50 ms) in the presence of picrotoxin induce recurrent activity during the second pulse. Therefore, a decrease in the ratio of the fEPSPs (response 2/ response 1) observed at DGKθ KO synapses might not actually reflect a change in the calcium-induced facilitation but rather a decrease in the recurrent activity induced in the second pulse. Qualitative comparison of recurrent activity induced during the second pulse of PPF measured at short ISIs showed that DGKθ KO synapses displayed less recurrent activity compared to WT (**Figure 6.6B**, 50 ms interval, red arrow). While these data require further quantitative confirmation, it is intriguing that loss of DGKθ produces opposite, and unequal effects on PPF in the presence and absence of picrotoxin. These opposing trends in the data suggest that DGKθ modulates excitatory drive onto both excitatory and inhibitory neurons, likely via distinct mechanisms.

Figure 6.6

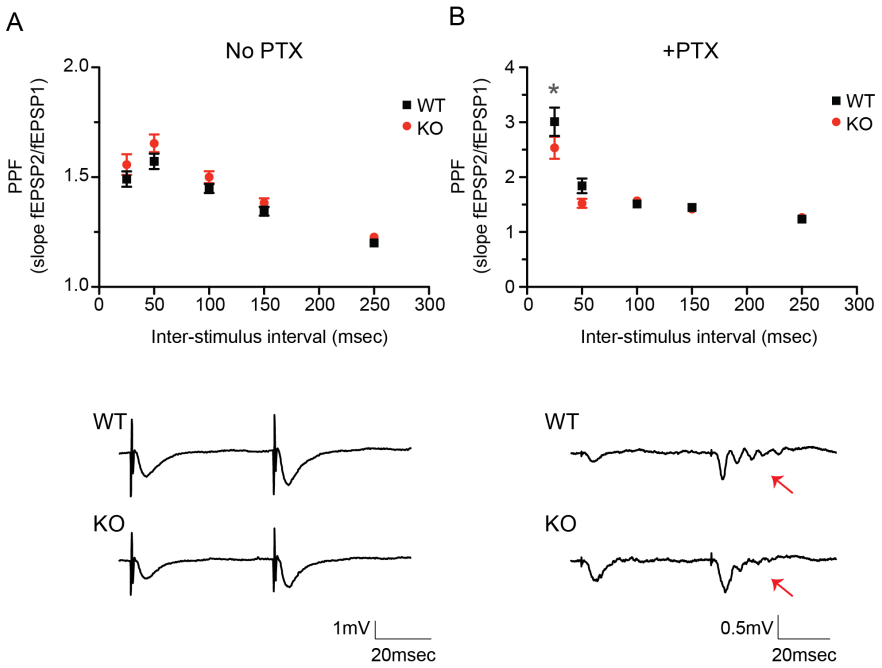

Figure 6.6. Acute slices from DGKθ KO mice display lower recurrent activity. Paired pulse facilitation (PPF) was assayed in acute hippocampal slices from WT and DGKθ KO mice in the absence (A) and presence (B) of picrotoxin (PTX). Top, the ratios of the paired-pulse response (fEPSP slope response 2 / fEPSP slope response 1) were plotted against the inter-stimulus intervals (in milliseconds, msec). Without PTX, when excitatory and inhibitory transmission is intact, PPF was not significantly different in DGKθ KO slices compared to WT (WT n=14, KO n=14; $p > 0.05$ at all inter-stimulus intervals, two-way repeated measures ANOVA with Bonferroni *post hoc* test). When PPF was assayed in the presence of 100 μM PTX (only excitatory transmission is intact, inhibitory transmission is blocked), DGKθ KO slices showed a significant decrease in facilitation with the shortest (25 msec) inter-stimulus interval (WT n=11, KO n=10; $p < 0.05$). Bottom, representative synaptic responses generated by a paired-pulse with a 50 msec inter-stimulus interval. KO slices showed less recurrent activity (red arrow) compared to WT during the second pulse. fEPSP – field excitatory postsynaptic potential.

Previous studies have shown that defects in SV recycling alter synaptic transmission by affecting the ability of the neurons to maintain neurotransmitter release during sustained neuronal activity (*18*, *60*, *62*, *63*). Since DGKθ KO neurons showed defect in SV retrieval following elevated neuronal activity (**Figure 5.3**), we speculated that evoked transmission could be attenuated in acute slices. To address this, we recorded field excitatory postsynaptic potentials (fEPSP) during a high frequency stimulus train (900 stimuli delivered at 50 Hz) in acute slices from WT and DGKθ KO SC-CA1 neurons. This stimulation successfully depressed synaptic transmission in both WT and KO synapses (**Figure 6.7A**). Comparison of the fEPSP amplitudes at the beginning (0-0.8 s) and end (17.6-18s) of the 50 Hz train with a two-way repeated measure ANOVA showed no significant difference between the two genotypes ($P_{0\text{-}0.4s} = 0.55$, n = 12/both; $P_{17.6\text{-}18s} = 0.80$, WT n = 10, KO n = 11, genotype effect, **Figures 6.7Ai-ii)**.

Since blockade of inhibitory transmission revealed a significant change in PPF in DGKθ KO slices, we speculated that the rate or amount of synaptic depression might also be affected in in the presence of picrotoxin compared to WT. Consistent with PPRs measured in the presence of picrotoxin (**Figure 6.6B**), DGKθ KO synapses exhibited a trend toward lower fEPSP amplitudes at the beginning of the 50 Hz train compared to WT ($P_{0\text{-}08s} = 0.33$, genotype effect, two way repeated measured ANOVA, WT n = 10, KO n = 9, **Figure 6.7Ai**). A similar trend towards lower fEPSP amplitudes was also observed at the end of the 50 Hz train at DGKθ KO synapses, however, this is likely not relevant since the synaptic responses at the end of the depleting stimulus train are very small and difficult to distinguish over the background electrical noise (($P_{17.3\text{-}17.98s} = 0.11$, genotype effect, WT n = 16, KO n = 12, **Figure 6.7Aii**).

Defects in SV recycling have also been shown to effect synaptic recovery following high frequency transmission (*60*, *64*, *65*). Despite showing no significant difference in the rate or degree of synaptic depression during the 50 Hz train, we speculated that DGKθ KO synapses might have altered synaptic transmission during the recovery period after the stimulus train is given. To address this, we measured field potentials at 2 Hz immediately following delivery of the depletion stimulus (900 AP, 50 Hz) in the presence and absence of picrotoxin. When excitatory and inhibitory transmission was intact (no picrotoxin), we measured a small decrease in the fEPSP amplitude of the first response measured at 2 Hz immediately following the 50 Hz train at DGKθ KO synapses compared to WT (**Figure 6.8B**). A two-tailed student's t test analysis of this first response found this decrease in fEPSP amplitude in DGKθ KO slices to be significant ($P = 0.037$, WT $n = 12$, KO $n = 12$). However, two-way repeated measure ANOVA shows that there is a significant effect of time on fEPSP amplitudes during the recovery ($P < 0.001$, time effect, $n = 12$/group). Therefore, while the student's t test is encouraging that this trend might be real (more experiments are necessary to validate this), is not an accurate measure of significance. When we used a repeated measures two-way ANOVA to compare of the first four responses of the 2 Hz recovery we found no significant difference in the fEPSP amplitudes between WT and DGKθ KO slices ($P = 0.176$, genotype effect, $n = 12$/group). While we currently lack enough data to form a firm conclusion of these data, the small decrease in fEPSP amplitude observed during the first response of the 2 Hz recovery is consistent with the defect in SV recycling measured at DGKθ KO synapses. When we repeated these experiments in the presence of picrotoxin, we observed an opposite trend in fEPSP amplitudes during the

first four responses of the 2 Hz recovery period (**Figure 6.7B**). DGKθ KO synapses showed slightly larger responses to the second and third recovery stimuli compared to WT, however, this difference did not reach statistical significance (P = 0. 116, genotype effect, two-way repeated measures ANOVA, n = 8/group).

Figure 6.7

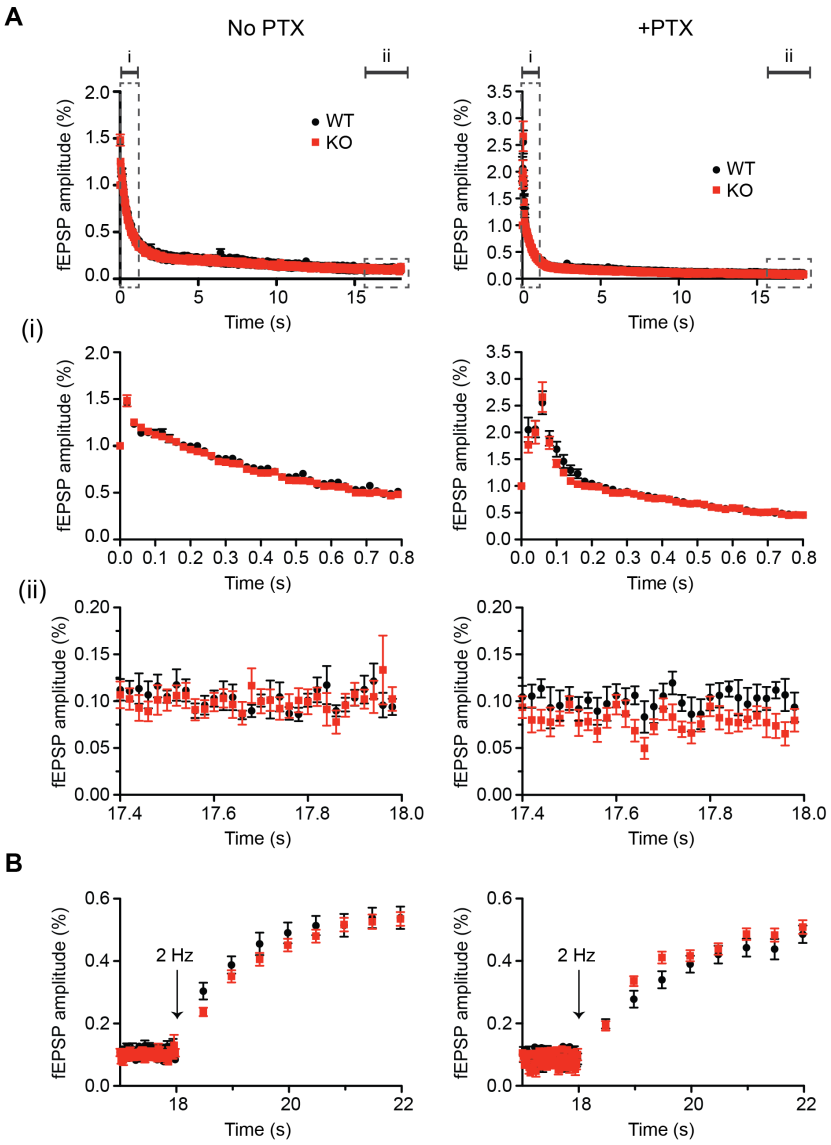

Figure 6.7. DGKθ KO mice show a small trend toward impaired synaptic recovery following high frequency stimulation. (A) Average amplitudes of fEPSPs measured in acute slices from WT and DGKθ KO mice during a high frequency stimulus train (900 stimuli, 50 Hz) were plotted against time (s). Responses from each slice were normalized to the peak fEPSP amplitude in the train. Top panel, average fEPSPs measured over the entire 50 Hz train in the absence (left) and presence (right) of 100 μM picrotoxin (PTX). Detailed view of fEPSPs during the beginning (i) and end (ii) of the stimulus train are shown below. Two-way repeated measures ANOVA with Bonferroni *post hoc* test found no significant difference between WT and DGKθ KO fEPSP amplitudes measured in the presence or absence of PTX ($p > 0.05$ interaction effect and at all time points, P values reported in text). (B) Synaptic recovery was probed in WT and DGKθ KO slices at 2 Hz (arrow) immediately following the 50 Hz stimulus train in the presence (right) and absence (left) of PTX. Two-way repeated measures ANOVA with Bonferroni *post hoc* test found no significant difference in recovery between WT and DGKθ KO ($p > 0.05$ at all individual time points, +/- PTX, summary P values reported in text).

While these data are complicated to interpret, together they demonstrate trends in altered transmission in DGKθ KO animals that could be explained by several different mechanisms. One possibility for the opposing DGKθ KO transmission phenotypes measured in the presence or absence of picrotoxin could be that DGKθ acts at glutamatergic synapses projecting onto both excitatory and inhibitory neurons. In the absence of DGKθ, glutamatergic drive from CA3 SC is decreased onto both CA1 pyramidal neurons and CA1 interneurons, meaning that overall synaptic transmission appears mostly intact. When inhibitory transmission is blocked with picrotoxin, the decreased excitatory drive onto excitatory neurons is revealed. While more experiments are necessary to provide data to support this hypothesis, analysis of the input-output data (I-O curves) already acquired during experiment's discussed here could be informative and should be explored in the future.

There are several possible explanations for the observed decrease in recurrent activity observed at KO SC-CA1 synapses: change in connectivity, difference in the number of synapses, number of excitatory and inhibitory synapses (E/I balance), or change in intrinsic excitability of the neurons. Many interesting questions emerge form these experiments. Is the altered recurrent activity in DGKθ KO animals a product of defective SV recycling over the course of development? Or is this a separate phenotype in the DGKθ KO mince due additional roles for DGKθ in neuronal tissue? Future experiments addressing these questions will help specify the physiologic role for DGKθ in the brain.

CHAPTER 7.

DISCUSSION

Despite speculations regarding the roles of mammalian DGKs in modulating synaptic function, the function of DGKθ in the brain has remained unknown. The data presented in this thesis were designed to test the hypothesis that DGKθ modulates neurotransmitter release from central synapses. I found that DGKθ protein expression is coincident with synaptogenesis and localizes specifically to excitatory synapses. Both acute and chronic loss of DGKθ from cortical neurons resulted in slowed SV retrieval following neuronal stimulation. SV recycling kinetics could be rescued by ectopic expression of enzymatically active, but not inactive, DGKθ, thus, implicating DGKθ catalytic activity in promoting the efficient recycling of SVs following neuronal activity.

7.1 DAG, DGKs and SV exocytosis

DGKs catalyze the conversion of DAG to PtdOH, thus, depletion of DGKθ is predicted to increase DAG levels, a lipid that has an established role in promoting SV exocytosis. This was observed in *C. elegans*, where loss of function mutation in the DGKθ homolog, DGK-1, produced elevated DAG which enhanced UNC13-mediated NT release from NMJ (*37*). Therefore, we were surprised when we found that depletion of DGKθ attenuated glutamate release from cortical neurons with no measurable change in the size of the recycling pool of SVs or the rate of SV exocytosis (**Figure 5.4).** While we have yet to measure synaptic DAG/PtdOH levels in DGKθ KO tissue, our studies indicate that DGKθ may not be the enzyme responsible for metabolizing DAG used for SV exocytosis, but rather may play a more important role in producing PtdOH used for SV retrieval.

If DGKθ is not the enzyme that clears exocytic pools of DAG, how is this lipid metabolized? Of the DGK isoforms found at excitatory presynaptic terminals, DGKι is

the mostly likely candidate for this role. DGKι is one of two type IV DGKs, localized to both pre- and postsynaptic sides of excitatory and inhibitory synapses, and is the only other DGK that has been shown to regulate a presynaptic function (*32*). Yang *et al.* found that DGKι knock-out mice displayed small increase in presynaptic release probability and a reduction in mGluR-LTD in young mice at an age when this processes is regulated by the presynaptic terminal (~2 weeks). While these findings implicate DGKι in the regulation of SV exocytosis, the activity of this isoform, alone, may not fully account for DAG-mediated potentiation of NT release, as loss of DGKι did not produce a significant change in PDBu-dependent potentiation of presynaptic release compared to WT animals(*32*). Previous work has shown that different signaling pathways are employed to enhance neurotransmission depending on the duration of PDBu treatment (*27*, *66*) prior to the stimulus. Both loss-of-function studies on DGKι and DGKθ have been performed in animals from a conventional KO background. If the prediction is correct and loss of DGK produces elevated DAG levels, both DGKι and DGKθ KO animals should have chronically elevated DAG levels during neurodevelopment and synaptogenesis. Thus, the stimulatory effect of PDBu will likely be different in these animals than those reported in WT backgrounds. Furthermore, loss of one DGK might be insufficient to elevate endogenous DAG levels those mimicked by PDBu-treatment. Future studies examining the effects of loss of two presynaptic kinases (DGKθ and DGKι) on presynaptic function will be very informative regarding the functional interaction and potential redundancy of these enzymes within a single subcellular compartment.

More work is needed to elucidate the precise role of DGKs in SV recycling during excitatory synaptic transmission. It is possible that DGKθ, DGKι, and other presynaptic

DGKs may have different activities depending on the strength and duration of the stimulus. Studies comparing SV recycling kinetics in DGKθ, DGKι, or both enzymes on SV cycling kinetics during various types of synaptic transmission roles will be informative.

With multiple DGK isoforms acting within the presynaptic terminal, it is unlikely that they are regulating one common pool DAG/PtdOH. Rather, we propose that DGKθ, DGKι, and other presynaptic DGKs are regulating distinct pools of these signaling lipids. Since SV exo- and endocytosis occur at spatially segregated sites within the bouton, we would predict that DGKι regulates DAG/PtdOH inside the active zone, at sites corresponding to vesicle release, and DGKθ regulates these lipids at adjacent regions (periactive zone) corresponding to sites of vesicle retrieval and endocytosis. Recent advances in microscopy techniques using super-resolution imaging, will likely permit the visualization of the dynamics of these individual lipid domains within the presynaptic membrane, in live cells.

The possibility that increases in one of the seven other neuronal DGK isoforms may compensate for the loss of DGKθ has not been completely ruled out. However, we were able to measure a significant reduction in DGK activity measured in DGKθ KO brain tissue and no change in protein expression of other DGK isoforms (**Figure 5C**). These data strongly argue against the notion that other DGK isoforms compensate for the loss DGKθ, and favor the idea that DGKθ plays a unique role in endocytosis. Future studies specifying the roles for other DGKs in SV recycling will provide further insight into the distinct or redundant roles of DGKs in presynaptic function.

7.2 DGKθ and PtdOH may regulate multiple endocytic retrieval pathways

If DGKθ is regulating a distinct pool of DAG that does not mediate SV exocytosis, it raises the intriguing possibility that it is the PtdOH produced by DGKθ, rather than its consumption of DAG, that is mediating its role in SV recycling. Two major pathways currently recognized to retrieve SVs from the plasma membrane in central nerve terminals are clathrin-mediated endocytosis (CME) and activity-dependent bulk endocytosis (ADBE). DGKθ appears to play a more critical role in promoting efficient retrieval of SVs during periods of sustained neuronal activity, when more action potentials are fired (**Figure 5.3)**. As ADBE is the dominant mechanism of SV retrieval during periods of intense neuronal activity, it is possible that DGKθ-mediated PtdOH production is involved in regulating ADBE. However, a recent unpublished study found that sypHy only reports on CME, not ADBE (unpublished observation, J.C. Nicholson-Fish et al. SFN 2014). It is clear, therefore, that we cannot exclude the possibility that DGKθ regulates ADBE and more experiments are necessary to place DGKθ in this pathway. SV recycling assays using FM1-43 and FM2-10 or the new pHluorin construct that does report on ADBE (unpublished observation, J.C. Nicholson-Fish et al. SFN 2014), will be critical to refine the signaling pathways regulated by DGKθ.

CME is the dominant mechanism of SV retrieval during mild neuronal activity and in such, is thought to be the dominant pathway employed during most modes of synaptic transmission *in vivo* (*11*, *16*, *53*). Since SV recycling kinetics were measured using sypHy, we may conclude that CME is slower in DGKθ KO neurons. Consistent with these data, previous studies in non-neuronal cells have shown that PtdOH production by DGKs is important for CME (*30*, *67*, *68*). However, DGK-mediated

PtdOH production has yet to be implicated in CME at central synapses. These studies, together with the data presented in this thesis, which demonstrate that DGKθ catalytic activity is required for its regulation of SV recycling, are the first to implicate DGKθ-mediated production of PtdOH in clathrin-mediated endocytosis of SVs.

While it is still unknown which proteins interact with DGKθ at synapses, previous studies in non-neuronal cells as well as *in vitro*, have shown that the small GTPase, RhoA, binds to DGKθ and inhibits its catalytic activity (*39*, *44*). Other DGK isoforms have been shown to interact with clathrin adaptors via conserved protein domains found in all DGK family members (*67*, *68*). Further studies are needed to elucidate the mechanisms by which DGKθ and possibly its production of PtdOH modulates the kinetics of SV recycling.

7.3 DGKθ, PtdOH, and synaptic PtdIns cycle

PtdOH is known to stimulate the activity of PIPK1γ, the major enzyme responsible for synaptic PtdIns(4,5)P_2 production (*63*, *69*). PtdIns(4,5)P_2 acts as an anchor for endocytic machinery in the synaptic plasma membrane (*2*, *20*, *68*). In addition to its regulation of PIPK1γ activity, PtdOH is also known to stimulate the activity of dynamin, the large GTPase responsible for pinching off internalized SVs (*20*, *21*). Thus, the reduction of DGKθ activity measured in KO tissue could result in a decrease in synaptic PtdOH, and, subsequently a reduction in PtdIns(4,5)P_2, leading to impaired recruitment of endocytic machinery and slowed SV endocytosis. Future studies elucidating the role of PtdOH in this cycle are necessary to determine if PtdOH is required primarily for PtdIns synthesis or as allosteric activator of PIPK1γ, dynamin I or other endocytic proteins that have an affinity for acidic phospholipids.

7.4 DGKs regulation of cellular trafficking in non-neuronal cells

DGKθ is not the first DGK to be implicated in regulating cellular trafficking and clathrin-mediated endocytosis. In non-neuronal cells, DGKζ and DGKδ have been shown to interact with CME adaptor proteins and thereby modulating receptor internalization and recycling (*67*, *68*, *70*). Interestingly, kinase-independent functions of DGKζ have been reported for this isoform in neuronal outgrowth (*71*). These studies together with our data suggest that DGK-modulation of membrane trafficking at neuronal synapses may be two-fold-(1) through catalytically-dependent DAG metabolism and (2) through catalytically-independent modulation of adaptor functions. DGKθ could be a good model to elucidate the adaptor functions of DGKs in cellular trafficking from the catalytic functions because, as mentioned previously, its catalytic activity is highly sensitive to mutations or truncations and it has multiple adaptor domains (*39*). While we show that DGKθ activity is required for its regulation of SV recycling, the abundance of protein-protein and protein-lipid domains in its primary amino acid sequence suggest that it could employ additional adaptor functions. As discussed above, many proteins involved in SV retrieval interact with one another via SH3 domains (Chapter 6.1) (*56*). If DGKθ is interacting with the endocytic machinery via its PRD or putative SH3-domain within the PRD, we would predict that the T6 truncation mutant, missing the N-terminal aa1-25 but with full catalytic activity, may not be able to recovery the defect in SV recycling observed in DGKθ KO neurons. Future experiments testing this hypothesis, as well as identifying endogenous interacting partners of DGKθ will provide valuable insight regarding the molecular mechanism behind DGKθ regulation of SV recycling.

Final remarks

While the balance of activity-induced SV exo- and endocytic processes is necessary to support synaptic transmission (*6*, *13*), recent work has shown that uncoupling of these two processes does not result in absolute failure of the opposing process (*72*-*74*). With nine DGK isoforms found in neuronal tissue in addition to the PLD family of enzymes, there are many possible routes available to neurons to ensure proper regulation of PtdOH, and, subsequently, PtdIns lipids in synaptic membranes. These data, together with our data showing opposing effects of picrotoxin on excitatory transmission in DGKθ KO slices suggest that neuronal signaling defects resulting from loss of DGKθ activity are balanced in the CNS. Thus, I hypothesize that the ability of the nervous system to compensate for such critical pathways, such as those mediating changes in neuronal lipid metabolism, is vital for the normal nervous system function and protection from of disease and dysfunction. Future experiments that assess alternative physiological deficits in DGKθ animals as well as behavioral outcomes will be exciting to pursue and will lend support for this hypothesis.

BIBLIOGRAPHY

1. D. Piomelli, G. Astarita, R. Rapaka, A neuroscientist's guide to lipidomics. *Nat Rev Neurosci* **8**, 743–754 (2007).

2. M. Koch, M. Holt, Coupling exo- and endocytosis: an essential role for PIP_2 at the synapse. *Biochim. Biophys. Acta* **1821**, 1114–1132 (2012).

3. D. Puchkov, V. Haucke, Greasing the synaptic vesicle cycle by membrane lipids. *Trends in Cell Biology* **23**, 493–503 (2013).

4. K. Bozek *et al.*, Organization and evolution of brain lipidome revealed by large-scale analysis of human, chimpanzee, macaque, and mouse tissues. *Neuron* **85**, 695–702 (2015).

5. J. Rohrbough, K. Broadie, Lipid regulation of the synaptic vesicle cycle. *Nat Rev Neurosci* **6**, 139–150 (2005).

6. V. Haucke, E. Neher, S. J. Sigrist, Protein scaffolds in the coupling of synaptic exocytosis and endocytosis. *Nat Rev Neurosci* **12**, 127–138 (2011).

7. G. Di Paolo *et al.*, Impaired PtdIns(4,5)P2 synthesis in nerve terminals produces defects in synaptic vesicle trafficking. *Nature* **431**, 415–422 (2004).

8. S. J. Royle, L. Lagnado, Clathrin-mediated endocytosis at the synaptic terminal: bridging the gap between physiology and molecules. *Traffic* **11**, 1489–1497 (2010).

9. B. G. Wilhelm *et al.*, Composition of isolated synaptic boutons reveals the amounts of vesicle trafficking proteins. *Science* **344**, 1023–1028 (2014).

10. N. L. Kononenko, V. Haucke, Molecular mechanisms of presynaptic membrane retrieval and synaptic vesicle reformation. *Neuron* **85**, 484–496 (2015).

11. G. Cheung, O. J. Jupp, M. A. Cousin, Activity-dependent bulk endocytosis and clathrin-dependent endocytosis replenish specific synaptic vesicle pools in central nerve terminals. *J. Neurosci.* **30**, 8151–8161 (2010).

12. E. T. Kavalali, Synaptic vesicle reuse and its implications. *Neuroscientist* **12**, 57–66 (2006).

13. T. C. Südhof, The synaptic vesicle cycle. *Annu. Rev. Neurosci.* **27**, 509–547 (2004).

14. N. Brose, C. Rosenmund, J. Rettig, Regulation of transmitter release by Unc-13 and its homologues. *Curr. Opin. Neurobiol.* **10**, 303–311 (2000).

15. S. Watanabe *et al.*, Ultrafast endocytosis at mouse hippocampal synapses. *Nature* **504**, 242–247 (2013).

16. E. L. Clayton, M. A. Cousin, The molecular physiology of activity-dependent bulk endocytosis of synaptic vesicles. *Journal of Neurochemistry* **111**, 901–914 (2009).

17. M. Mani *et al.*, The Dual Phosphatase Activity of Synaptojanin1 Is Required for Both Efficient Synaptic Vesicle Endocytosis and Reavailability at Nerve Terminals. *Neuron* **56**, 1004–1018 (2007).

18. O. Cremona *et al.*, Essential role of phosphoinositide metabolism in synaptic vesicle recycling. *Cell* **99**, 179–188 (1999).

19. E. R. Chapman, How does synaptotagmin trigger neurotransmitter release? *Annu. Rev. Biochem.* **77**, 615–641 (2008).

20. K. N. Burger, R. A. Demel, S. L. Schmid, B. de Kruijff, Dynamin is membrane-active: lipid insertion is induced by phosphoinositides and phosphatidic acid. *Biochemistry* **39**, 12485–12493 (2000).

21. J. Zheng *et al.*, Identification of the binding site for acidic phospholipids on the pH domain of dynamin: implications for stimulation of GTPase activity. *J. Mol. Biol.* **255**, 14–21 (1996).

22. B. Tu-Sekine, D. M. Raben, Regulation and roles of neuronal diacylglycerol kinases: a lipid perspective. *Critical Reviews in Biochemistry and Molecular Biology* **46**, 353–364 (2011).

23. J. Basu, A. Betz, N. Brose, C. Rosenmund, Munc13-1 C1 domain activation lowers the energy barrier for synaptic vesicle fusion. *J. Neurosci.* **27**, 1200–1210 (2007).

24. C. S. Bauer, R. J. Woolley, A. G. Teschemacher, E. P. Seward, Potentiation of exocytosis by phospholipase C-coupled G-protein-coupled receptors requires the priming protein Munc13-1. *J. Neurosci.* **27**, 212–219 (2007).

25. I. Augustin, C. Rosenmund, T. C. Südhof, N. Brose, Munc13-1 is essential for fusion competence of glutamatergic synaptic vesicles. *Nature* **400**, 457–461 (1999).

26. F. Varoqueaux *et al.*, Total arrest of spontaneous and evoked synaptic transmission but normal synaptogenesis in the absence of Munc13-mediated vesicle priming. *Proc. Natl. Acad. Sci. U.S.A.* **99**, 9037–9042 (2002).

27. J. S. Rhee *et al.*, Beta phorbol ester- and diacylglycerol-induced augmentation of transmitter release is mediated by Munc13s and not by PKCs. *Cell* **108**, 121–133 (2002).

28. J. W. Barclay, Munc-18-1 regulates the initial release rate of exocytosis. *Biophys. J.* **94**, 1084–1093 (2008).

29. I. Mérida, A. Avila-Flores, E. Merino, Diacylglycerol kinases: at the hub of cell signalling. *Biochem. J.* **409**, 1–18 (2008).

30. C. N. Antonescu, G. Danuser, S. L. Schmid, Phosphatidic acid plays a regulatory role in clathrin-mediated endocytosis. *Mol. Biol. Cell* **21**, 2944–2952 (2010).

31. B. Luo, S. M. Prescott, M. K. Topham, Diacylglycerol kinase zeta regulates phosphatidylinositol 4-phosphate 5-kinase Ialpha by a novel mechanism. *Cell. Signal.* **16**, 891–897 (2004).

32. J. Yang *et al.*, DGKι regulates presynaptic release during mGluR-dependent LTD. *The EMBO Journal* **30**, 165–180 (2011).

33. K. Kim, J. Yang, E. Kim, Diacylglycerol kinases in the regulation of dendritic spines. *Journal of Neurochemistry* **112**, 577–587 (2010).

34. K. Kakefuda *et al.*, Diacylglycerol kinase β knockout mice exhibit lithium-sensitive behavioral abnormalities. *PLoS ONE* **5**, e13447 (2010).

35. A. Musto, N. G. Bazan, Diacylglycerol kinase epsilon modulates rapid kindling epileptogenesis. *Epilepsia* **47**, 267–276 (2006).

36. Y. Shirai *et al.*, Essential role of neuron-enriched diacylglycerol kinase (DGK), DGKbeta in neurite spine formation, contributing to cognitive function. *PLoS ONE* **5**, e11602 (2010).

37. S. Nurrish, L. Ségalat, J. M. Kaplan, Serotonin inhibition of synaptic transmission: Galpha(0) decreases the abundance of UNC-13 at release sites. *Neuron* **24**, 231–242 (1999).

38. G. Baldanzi *et al.*, Negative regulation of diacylglycerol kinase theta mediates adenosine-dependent hepatocyte preconditioning. *Cell Death and Differentiation* **17**, 1059–1068 (2010).

39. A. P. Los, J. van Baal, J. de Widt, N. Divecha, W. J. van Blitterswijk, Structure-activity relationship of diacylglycerol kinase theta. *Biochim. Biophys. Acta* **1636**, 169–174 (2004).

40. V. Anggono, R. L. Clem, R. L. Huganir, PICK1 loss of function occludes homeostatic synaptic scaling. *J. Neurosci.* **31**, 2188–2196 (2011).

41. B. Tu-Sekine, D. M. Raben, Dual regulation of diacylglycerol kinase (DGK)-θ: polybasic proteins promote activation by phospholipids and increase substrate affinity. *Journal of Biological Chemistry* **287**, 41619–41627 (2012).

42. S. Ueda, B. Tu-Sekine, M. Yamanoue, D. M. Raben, Y. Shirai, The expression of diacylglycerol kinase theta during the organogenesis of mouse embryos. *BMC Dev. Biol.* **13**, 35 (2013).

43. B. Houssa *et al.*, Cloning of a novel human diacylglycerol kinase (DGKtheta) containing three cysteine-rich domains, a proline-rich region, and a pleckstrin homology domain with an overlapping Ras-associating domain. *J. Biol. Chem.* **272**, 10422–10428 (1997).

44. B. Houssa, J. de Widt, O. Kranenburg, W. H. Moolenaar, W. J. van Blitterswijk, Diacylglycerol kinase theta binds to and is negatively regulated by active RhoA. *J. Biol. Chem.* **274**, 6820–6822 (1999).

45. G. Tabellini *et al.*, Diacylglycerol kinase-theta is localized in the speckle domains of the nucleus. *Exp. Cell Res.* **287**, 143–154 (2003).

46. G. Tabellini *et al.*, Nuclear diacylglycerol kinase-theta is activated in response to nerve growth factor stimulation of PC12 cells. *Cell. Signal.* **16**, 1263–1271 (2004).

47. B. Tu-Sekine, H. Goldschmidt, E. Petro, D. M. Raben, Diacylglycerol kinase θ: regulation and stability. *Advances in Biological Regulation* **53**, 118–126 (2013).

48. E. Eden *et al.*, Proteome half-life dynamics in living human cells. *Science* **331**, 764–768 (2011).

49. B. Granseth, B. Odermatt, S. J. Royle, L. Lagnado, Clathrin-mediated endocytosis is the dominant mechanism of vesicle retrieval at hippocampal synapses. *Neuron* **51**, 773–786 (2006).

50. S. Sankaranarayanan, T. A. Ryan, Real-time measurements of vesicle-SNARE recycling in synapses of the central nervous system. *Nat Cell Biol* **2**, 197–204 (2000).

51. S. Sankaranarayanan, D. De Angelis, J. E. Rothman, T. A. Ryan, The use of pHluorins for optical measurements of presynaptic activity. *Biophys. J.* **79**, 2199–2208 (2000).

52. W. C. Skarnes *et al.*, A conditional knockout resource for the genome-wide study of mouse gene function. *Nature* **474**, 337–342 (2011).

53. E. L. Clayton, M. A. Cousin, Differential labelling of bulk endocytosis in nerve terminals by FM dyes. *Neurochem. Int.* **53**, 51–55 (2008).

54. T. Fernández-Alfonso, T. A. Ryan, The kinetics of synaptic vesicle pool depletion at CNS synaptic terminals. *Neuron* **41**, 943–953 (2004).

55. S. Sankaranarayanan, T. A. Ryan, Calcium accelerates endocytosis of vSNAREs at hippocampal synapses. *Nat. Neurosci.* **4**, 129–136 (2001).

56. V. Anggono, P. J. Robinson, Syndapin I and endophilin I bind overlapping proline-rich regions of dynamin I: role in synaptic vesicle endocytosis. *Journal of Neurochemistry* **102**, 931–943 (2007).

57. Y. Wu *et al.*, A dynamin 1-, dynamin 3- and clathrin-independent pathway of synaptic vesicle recycling mediated by bulk endocytosis. *eLife* **3**, e01621 (2014).

58. S. M. Ferguson *et al.*, A selective activity-dependent requirement for dynamin 1 in synaptic vesicle endocytosis. *Science* **316**, 570–574 (2007).

59. A. Raimondi *et al.*, Overlapping role of dynamin isoforms in synaptic vesicle endocytosis. *Neuron* **70**, 1100–1114 (2011).

60. K. J. Vargas *et al.*, Synucleins regulate the kinetics of synaptic vesicle endocytosis. *J. Neurosci.* **34**, 9364–9376 (2014).

61. S. M. Ferguson *et al.*, A Selective Activity-Dependent Requirement for Dynamin 1 in Synaptic Vesicle Endocytosis. *Science* **316**, 570–574 (2007).

62. H. Zhao *et al.*, SCAMP5 plays a critical role in synaptic vesicle endocytosis during high neuronal activity. *J. Neurosci.* **34**, 10085–10095 (2014).

63. M. R. Wenk *et al.*, PIP kinase Igamma is the major PI(4,5)P(2) synthesizing enzyme at the synapse. *Neuron* **32**, 79–88 (2001).

64. A. J. Newton, T. Kirchhausen, V. N. Murthy, Inhibition of dynamin completely blocks compensatory synaptic vesicle endocytosis. *Proc. Natl. Acad. Sci. U.S.A.* **103**, 17955–17960 (2006).

65. S. E. Kwon, E. R. Chapman, Synaptophysin regulates the kinetics of synaptic vesicle endocytosis in central neurons. *Neuron* **70**, 847–854 (2011).

66. K. D. B. Wierda, R. F. G. Toonen, H. de Wit, A. B. Brussaard, M. Verhage, Interdependence of PKC-dependent and PKC-independent pathways for presynaptic plasticity. *Neuron* **54**, 275–290 (2007).

67. C. D. Nelson *et al.*, Targeting of diacylglycerol degradation to M1 muscarinic receptors by beta-arrestins. *Science* **315**, 663–666 (2007).

68. T. Kawasaki, T. Kobayashi, T. Ueyama, Y. Shirai, N. Saito, Regulation of clathrin-dependent endocytosis by diacylglycerol kinase delta: importance of kinase activity and binding to AP2alpha. *Biochem. J.* **409**, 471–479 (2008).

69. H. Ishihara *et al.*, Type I phosphatidylinositol-4-phosphate 5-kinases. Cloning of the third isoform and deletion/substitution analysis of members of this novel lipid kinase family. *J. Biol. Chem.* **273**, 8741–8748 (1998).

70. J. Cai *et al.*, Diacylglycerol kinase delta and protein kinase C(alpha) modulate

epidermal growth factor receptor abundance and degradation through ubiquitin-specific protease 8. *Journal of Biological Chemistry* **285**, 6952–6959 (2010).

71. Y. Yakubchyk *et al.*, Regulation of neurite outgrowth in N1E-115 cells through PDZ-mediated recruitment of diacylglycerol kinase zeta. *Mol. Cell. Biol.* **25**, 7289–7302 (2005).

72. T. L. Schwarz, Synaptotagmin promotes both vesicle fusion and recycling. *Proc. Natl. Acad. Sci. U.S.A.* **101**, 16401–16402 (2004).

73. K. Nicholson-Tomishima, T. A. Ryan, Kinetic efficiency of endocytosis at mammalian CNS synapses requires synaptotagmin I. *Proc. Natl. Acad. Sci. U.S.A.* **101**, 16648–16652 (2004).

74. J. Yao, S. E. Kwon, J. D. Gaffaney, F. M. Dunning, E. R. Chapman, Uncoupling the roles of synaptotagmin I during endo- and exocytosis of synaptic vesicles. *Nat. Neurosci.* **15**, 243–249 (2012).

CURRICULUM VITAE

HANA LEAH GOLDSCHMIDT

2735 N Calvert Street, #1 hgoldsc1@jhmi.edu
Baltimore, Maryland, 21218 (510) 910-0768

EDUCATION

Ph.D.	2009-*present*	Program in Biochemistry, Cellular and Molecular Biology (BCMB), Department of Biological Chemistry, Johns Hopkins University School of Medicine (JHU SOM), Baltimore, MD U.S.A Mentor: Daniel M. Raben, Ph.D., and Richard L. Huganir, Ph.D Thesis Focus: Determine the role of diacylglycerol kinase-θ (DGKθ) in the regulation of synaptic vesicle recycling at central nerve terminals. *Anticipated graduation April 2015*
B.A.	2003-2007	Biochemistry (Distinction) *Cum Laude*; Minor, Spanish Occidental College, Los Angeles, CA U.S.A Mentor: Chris Craney, M.S., D.A. Senior Thesis: Antibodies Need Sugar- The Importance of Glycosylation in Immunoglobulin G Activity.
	2006	CIEE Study Abroad Program Universidad Católica de Valparaíso, Valparaíso, Chile

RESEARCH EXPERIENCE

Research Rotation	2010	Laboratory of Dr. James Stivers, Ph.D JHU SOM Department of Pharmacology and Molecular Sciences
Research Rotation	2010	Laboratory of Dr. Andrew Feinberg, M.D., M.P.H. JHU SOM Center for Epigenetics

Staff Research Associate I	2007-2009	Laboratory of Dr. Kevin Shannon, M.D., University of California, San Francisco, San Francisco, CA Department of Pediatrics Project Title: "Dissecting Aberrant Ras Signaling Induced by hyperactive Ras in Myeloid Diseases"
Undergraduate Researcher	2005-2007	Laboratory of Dr. Chris Craney, M.S., D.A. Occidental College, Los Angeles, CA Department of Biochemistry Project Title: "The Role of the Glucose-6-Phosphate Dehydrogenase Dimer Interface: Proteolytic Studies"

PUBLICATIONS

Goldschmidt, H.L., Tu-Sekine, B., Volk, L., Anggono, V, Huganir, R.L. and Raben, D.M. DGKθ activity regulates the kinetics of SV recycling at central nerve terminals. *Manuscript submitted as a Brief Communication to the Journal of Neuroscience.*

Tu-Sekine, B., **Goldschmidt, H.** and Raben, D.M. (2015) Diacylglycerol, phosphatidic acid, and their metabolic enzymes in synaptic vesicle recycling. *Advances in Enzymology* 57, 147-152.

Diaz-Flores, E., **Goldschmidt, H.**, Depeille, P., Ng, V., Akutagawa, J., Krisman, K., Crone, M., Burgess, M.R., Williams,O., Houseman, B., Shokat, K., Sampath, D., Bollag, G., Roose, J.P., Braun, B.S. and Shannon, K.M. (2013) PLC-γ and PI3K link cytokines to ERK activation in hematopoietic cells with normal and oncogenic Kras. *Science Signaling* 6 (304), ra105.

Tu-Sekine, B., **Goldschmidt, H.**, Petro, E. and Raben, D.M. (2013) Diacylglycerol kinase θ: regulation and stability. *Advances in Enzymology* 53, 118-126.

Nabel, C.S., Jia, H., Ye, Y., Shen, L., **Goldschmidt, H.L.**, Stivers, J.T., Zhang,Y. and Kohli, R.M. (2012) AID/APOBEC deaminases disfavor modified cytosines implicated in DNA demethylation. *Nature Chemical Biology* 8 (9): 751-8.

MENTORSHIP/TEACHING EXPERIENCE

2013 Mentor for summer student Lucy Phillips.
Department of Biological Chemistry & Department of Neuroscience, JHUSOM
Successfully taught Lucy laboratory techniques important for my thesis project. Also, provided mentorship, support and guidance to help prepare Lucy to apply to Medical school.

2010-2013 Gradate Teaching Assistant
Organic mechanisms in biology, JHUSOM
Lead group tutorials and worked with first year BCMB graduate students individually to help them understand concepts taught in the course.

2013 Gradate Teaching Assistant
Effective Science Communication (Fall), JHUSOM
Assisted in course organization and homework assignment grading.

2010 & 2012 Graduate Teaching Assistant
Scientific Foundations of Medicine-Metabolism section, JHUSOM
Assisted Dr. Michael Wolfgang (2010) and Dr. Michael Caterina (2012) in leading a small discussion group for first year medical students. I helped students from diverse scientific backgrounds understand and apply concepts taught in class by working through problem sets for each lecture.

2005-2007 Workshop Leader
Academic Mastery Program, Occidental College, Los Angeles, CA
Organize challenging workshops for students taking organic chemistry at Occidental College by preparing worksheets and mock exams for the students. The purpose of the program is to provide a place for students to work collaboratively and intensively with peers and emphasize conceptual understanding of the material.

PRESENTATIONS

Goldschmidt, H.L., Tu-Sekine, B., Volk, L, Anggono, V, Huganir, R.L. and Raben, D.M. (2014) DGKθ at the Synapse: a role for the metabolism of DAG in synaptic vesicle recycling? **Poster Presentation.** BCMB program retreat, Harbourtowne, St. Michaels, MD, U.S.A, October 12-13, 2014.

Goldschmidt, H.L., Tu-Sekine, B., Anggono, V, Huganir, R.L. and Raben, D.M. (2013) DGKθ at the Synapse: a role for the metabolism of DAG in synaptic vesicle recycling? **Poster Presentation.** Argentine Society for Biochemistry and Molecular Biology Research Conference on Molecular mechanisms in cell signaling and gene expression, Buenos Aires, Argentina, November 6-7, 2013.

Goldschmidt, H.L., Tu-Sekine, B., Anggono, V, Huganir, R.L. and Raben, D.M. (2013) DGKθ at the Synapse: a role for the metabolism of DAG in synaptic vesicle recycling? **Oral Presentation.** BCMB program retreat, Harbourtowne, St. Michaels, MD, U.S.A, October 6-7, 2013.

Goldschmidt, H.L., Tu-Sekine, B., Anggono, V, Phillips, L., Huganir, R.L. and Raben, D.M. (2013). DGKθ at the Synapse: a role for the metabolism of DAG in synaptic vesicle recycling? **Poster Presentation.** Gordon Research Conference on Molecular & Cellular Biology of Lipids, Waterville Valley, NH, U.S.A, July 21-26, 2013.

Goldschmidt, H.L. and Craney, C. (2007). The critical role of the glucose-6-phosphate dehydrogenase dimer interface: proteolytic studies.. **Oral presentation**. 21st National Conference on Undergraduate Research, Dominican University, San Rafael, CA, U.S.A, April 12-14, 2007.

HONORS AND AWARDS

2007	Norris Science Research Fellowship
2006-2007	Student Representative, Chemistry Faculty Search Committee
2006	Howard Hughes Medical Institute Professional Apprenticeship Recipient
2006	C. David West Summer Research Fellow
2005	Sherman Fairchild Summer Research Fellowship Recipient